Available online at website: https://journal.bcrec.id/index.php/bcrec

Bulletin of Chemical Reaction Engineering & Catalysis, 21 (3) 2026, 617-637

Original Research Article

Improvements in Photocatalytic Activity in Visible Light Destruction of Chlorpyrifos in a Batch Reactor Applying the Z-Scheme g-C_3N_4/Fe_3O_4/$CuWO_4$/CuO Heterojunction, Including Fabrication, Characterization, and Recycling

Shno M. Ali[1,2], Abeer I. Alwared[1,*]

[1]Environmental Engineering Department, College of Engineering, University of Baghdad, Baghdad, Iraq
[2]Civil Engineering Department, College of Engineering, University of Kirkuk, Kirkuk, Iraq.

Received: 29th March 2026; Revised: 16th April 2026; Accepted: 17th April 2026
Available online: 27th April 2026; Published regularly: October 2026

Abstract

The most widely used pesticide in agricultural regions across the entire globe is chlorpyrifos (CPF).In the present research, g-C_3N_4/Fe_3O_4/$CuWO_4$/CuO heterojunction has been created through a series of straightforward technologies and used for photocatalytic degradation of chlorpyrifos .The produced g-C_3N_4/Fe_3O_4/$CuWO_4$/CuO nanocomposites' optical and magnetic features, structure, and morphologies have been investigated using XRD, FTIR, elemental mapping, EDS, SEM, TEM, VSM, DRS, PL, and BET methodologies. With rate constants of 0.00507 and 0.00696 min^{-1}, correspondingly, the photocatalyst enabled the photocatalytic degradation of chlorpyrifos, g-C_3N_4, and $CuWO_4$, which achieved maximal efficiencies of 50% and 69% in visible light. However, under visible light, g-C_3N_4/Fe_3O_4/$CuWO_4$/CuO exhibited a maximum performance of 93% with rate constants of 0.0159 min^{-1}. In order to remove chlorpyrifos from aqueous solution, this work created a unique type of g-C_3N_4/Fe_3O_4/$CuWO_4$/CuO nanocomposite utilizing a multistage procedure using a photocatalytic technique employing novel catalysts. Being exposed to visible light, the as-fabricated g-C_3N_4/Fe_3O_4/$CuWO_4$/CuO substantially enhanced the photocatalytic activity for the successful elimination of pesticide, boosting its potential for use in ecologically friendly water purification systems.

Keywords: Water purification; Z- scheme; Reusability; Chlorpyrifos pesticide; Visible light

How to Cite: Ali, S. M., Alwared, A. I. (2026). Improvements in Photocatalytic Activity in Visible Light Destruction of Chlorpyrifos in a Batch Reactor Applying the Z-Scheme g-C_3N_4/Fe_3O_4/CuWO4/CuO Heterojunction, Including Fabrication, Characterization, and Recycling. *Bulletin of Chemical Reaction Engineering & Catalysis*, 21 (3), 617-637. (DOI: 10.9767/bcrec.20698)

Permalink/DOI: https://doi.org/10.9767/bcrec.20698

1. Introduction

The organophosphorus pesticides have been identified by their excellent water solubility and their ability to contaminate groundwater by permeating deeply into the soil [1]. One popular organophosphate insecticide in agriculture is chlorpyrifos, an irreversible cholinesterase inhibitory [2]. However, being forbidden for usage at home, the majority of chlorpyrifos substances are nevertheless employed in the kitchen, washroom, and agricultural fields [3]. The quantity, duration, and frequency of exposure to chlorpyrifos influence its effects on human wellness [4]. Any aquatic creature is still at risk from the acute poisoning of chlorpyrifos [5]. As a direct result, outflow from urban streams and agricultural land has huge amounts of CPF [6]. Numerous approaches to eliminate chlorpyrifos from the environment are being considered because of the pesticide's multiple negative impacts on humans and ecological systems [7]. Environmental studies and the removal of

* Corresponding Authors.
Email: dr.Abeer.wared@coeng.uobaghdad.edu.iq (A.I. Alwared)

harmful substances from aqueous solutions are two areas of major interest due to the constantly increasing uses of nanomaterial developments [8].In response to environmental degradation and shortages of energy in recent decades, photocatalytic technique has attracted a lot of attention as well as application [9]. To cure different impurities, a number of conventional approaches are utilized. Filtration, oxidation by chemicals, membrane filtering, crystallization, sedimentation, and other processes supply the foundation of these basic methods. These techniques have limitations since they are costlier and have lesser removal efficiency [10,11]. One of the AOPs is the photocatalysis process, which is regarded as an exciting technology among many water treatment techniques due to its high efficacy, cost-effectiveness and environmental friendliness, and recycling ability [12].

Heterogeneous photocatalysis has emerged as a successful approach among advanced oxidation procedures (AOPs) for the purification of various constituents from wastewater [13,14,15]. Highly reactive substances, primarily hydroxyl radicals (·OH), are created in situ during these procedures, permitting the highly refractory compounds to oxidize non-selectively to generate carbon dioxide, water, and additional inorganic ions [16,17]. Low bandgap semiconductors which includes Cu_2O, Bi_2S_3, $BiVO_4$, Fe_3O_4, WO_3, and $CuWO_4$ have been put forward by a number of scientists [18]. $CuWO_4$ is an n-type semiconductor within metal tungstates featuring an adequate bandgap of 2.2–2.4 eV and moderate toxicity that is utilized to offer enhanced photocatalytic capacity [19,20]. Due to its excellent visible light-driven photocatalyst for the elimination of chemical contaminants, copper tungstate ($CuWO_4$) has been extensively studied [21]. Due to its potential optical, electricity, and magnetic attributes, Fe_3O_4 has recently drawn the interest of several researchers. It can be coupled to other photocatalyst substances in a core-shell structure to develop a recoverable photocatalyst [22]. Fe_3O_4 (n-type, bandgap = 1.1–1.8 eV) has attracted a lot fascination in g-C_3N_4 alteration to enhance its optical, electrical, and photoelectrochemical features [23]. Because g-C_3N_4 is a special 2D layered nonmetallic material, it has excellent thermal stability, an easy fabrication procedure, and an energy band structure that makes it ideal for the photocatalytic degradation of water [24].In addition to their remarkable stability chemically, appropriate energetic band structure, and superior absorption of light, g-C_3N_4 has gained extensive usage in photocatalytic technology [25]. With a tunable power bandgap of roughly 2.7 eV, it is likewise cheap, harmless, defect-free, and adaptable to a wide range of pH circumstances, resulting in an excellent photocatalyst [26]. It has been the subject of multiple studies as the most fascinating visible-light-activated photocatalyst [27]. Nevertheless, pure g-C_3N_4's catalytic capability is inadequate for real-world use.It has been reported that doping with metal or non-metal ions or producing nanocomposites may improve g-C_3N_4's catalytic efficiency [28]. Between 1.2 and 2.1 eV, copper oxide (CuO) nanoparticles exhibit the highest and most indirect band gap among each of the metal and metal oxide nanoparticles [29]. CuO, a p-type small band gap (1.2 eV) semiconductor with perfect electrochemical and optical characteristics, cheap cost, and non-toxicity, is a standard instance that has been deeply studied [30]. When illuminated by visible light, CuO nanoparticles' remarkable photocatalytic features — such as their large surface area and sufficient bandgap energy — allow them to produce reactive oxygen species [31]. CuO nanoparticles can take on a range of morphological forms, such as ellipsoids, nanowires, nanoflowers, nanoplates, and nanoboats, which may dramatically impact the way they decompose organic contaminants in solution [32]. Due to its extensive use in agriculture, the pesticide chlorpyrifos was chosen as a pollutant because the discharged water runs off into surface water and contaminated groundwater, which is directly used for drinking in the neighboring towns in study region. With the goal to generate a novel Z-scheme form g-C_3N_4/Fe_3O_4/$CuWO_4$/CuO that enhances visible-light photocatalytic degradation of Chlorpyrifos from a solution of water, we adopted CuO p- type nanoparticles' and $CuWO_4$ n-type forms and precipitated it on g-C_3N_4/Fe_3O_4 nanocomposite. Nevertheless, neither the manufacturing process of the quaternary nanocomposite material g-C_3N_4/Fe_3O_4/$CuWO_4$/CuO nor its photocatalytic degradation of chlorpyrifos are known. thereby, the current study shows the way the quaternary nanocomposite material works in the photocatalytic elimination of chlorpyrifos.

2. Materials and Method

2.1 Chemicals and Reagents

Ferric chloride hexahydrate ($FeCl_3.6H_2O$, 97%), ferric chloride tetrahydrate ($FeCl_2.4H_2O$, 99%), tungstate of sodium dehydrated ($Na_2WO_4.2H_2O$, 98.0%), melamine ($C_3H_6N_6$, 99.0%), ethanol, which is (C_2H_5OH, 100%), Copper-nitrate-trihydrate ($Cu(NO_3)_2.3H_2O$, 98.0%), iso-propyl alcohol ($(CH_3)_2CHOH$), ethylenediaminetetraacetic acid disodium salt dehydrate (EDTA-2Na, $C_{10}H_{14}N_2Na_2O_8.2H_2O$, 99.0%), p-benzoquinone (BQ, $C_6H_4(=O)_2$, 99.0%), isopropanol (IPA, $(CH_3)_2CHOH$, 99.5%), sodium hydroxide (NaOH, 99.88%), and hydrochloric acid (HCl), chlorpyrifos ($C_9H_{11}Cl_3NO_3PS$, purity 99.8%). All of these substances were bought

through Thomas Baker in India without any further purification. Figure 1 show chemical structure of Chlorpyrifos, while Table 1 provides an outline of the physiochemical properties of the organic pollutant Chlorpyrifos (CPF) [33].

2.2 Fabrication of the Photocatalysts

The photocatalysts were manufactured in accordance with our earlier work [34]. 4 g of melamine was heated at 550 °C for 4 hours in a muffle oven using ambient pressure in order to produce bulk g-C_3N_4. The yellow compound being produced by the reaction was subsequently gathered for use later on [35]. g-C_3N_4/Fe_3O_4 (CNF) compounds have been produced by distributing 2 g of g-C_3N_4 in 200 mL of a blended solution including one ethanol and two water molecules, then undergoing two hours of ultrasound treatment. The previous solution was then heated to 60 °C and supplied with 0.22 g of $FeCl_2 \cdot 4H_2O$ and 0.46 g of $FeCl_3 \cdot 6H_2O$. The reaction mixture was subsequently diluted with 10 mL of water containing ammonia for 30 minutes at 80 °C, permitted to cool naturally, and then cleaned four times with deionized water to sterilize it. In accordance with [36], the nanocomposites have been dried at 65 °C. The hydrothermal approach was used to generate the g-C_3N_4/Fe_3O_4/$CuWO_4$ (CNFC) nanocomposite (Figure 2). First, 150 mL of water was employed to thoroughly disperse 0.35 g of the g-C_3N_4/Fe_3O_4 nanocomposite utilizing the ultrasonic method for a period of five minutes. Next, the g-C_3N_4/Fe_3O_4 suspension was mixed with 0.096 g of copper nitrate $Cu(NO_3)_2.3H_2O$ and left for 60 minutes. The beaker was next filled with 20 mL of an aqueous solution which included 0.158 g of sodium tungstate $Na_2WO_4.2H_2O$, and it was stirred periodically for 60 minutes. Aqueous sodium hydroxide (5 M) was progressively added to the suspension while stirring until the pH reached 8.3 and refluxed. The resulting substance was then moved to a 100 mL Teflon-lined autoclave and heated for two hours at 96 °C. The photocatalyst was then taken out, sanitized and calcined for three hours at 450 °C. The same technique was used for creating purely $CuWO_4$ without adding g-C_3N_4/ Fe_3O_4 nanocomposite [37]. The co-precipitation technique for generating g-C_3N_4/Fe_3O_4/$CuWO_4$/CuO was shown in Figure 2.

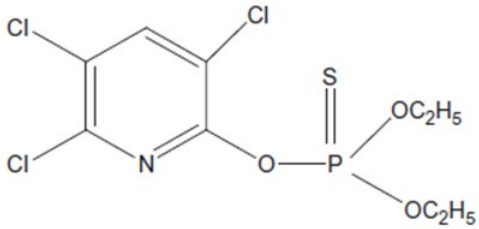

Figure 1. Chemical structure of Chlorpyrifos [33].

Table 1. Physiochemical characteristics of Chlorpyrifos [33].

Name	Chlorpyrifos
Empirical formula	$C_9H_{11}Cl_3NO_3PS$
Molecular weight (g/mol)	350.6
Water solubility (mg/L) at 25°C	2.0
Vapor pressure (mm Hg at 25°C)	2.7
Octanol water coeff. (Kow)	4.7–5.3
Melting point	41–43.5 °C
Density (g/cm^3)	1.398
Toxicity class	II

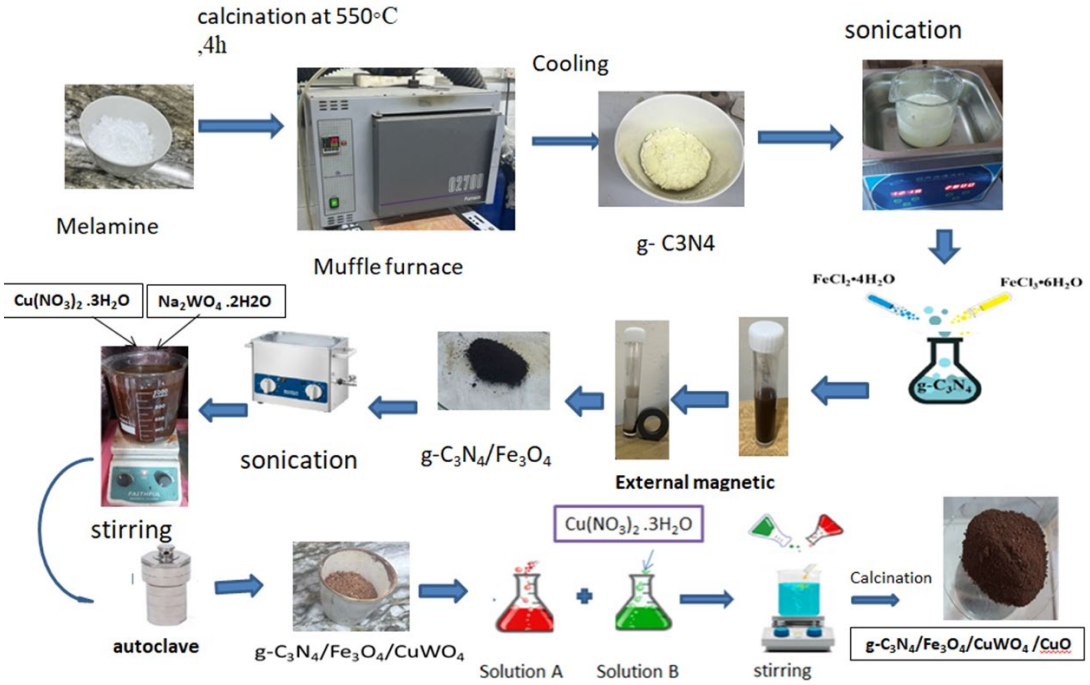

Figure 2. A schematic representation of a CNFCC process of manufacture.

Two grams of g-C_3N_4/Fe_3O_4/$CuWO_4$ are ultrasonically treated for five minutes to create solution A. After that, create solution B by adding 0.2 gram of $Cu(NO_3)_2.3H_2O$ to 250 mL of deionized water and waiting until the pH value reaches 5. The mixture is stirred for three hours at 90 degrees Celsius after solution B and solution A have been combined. Finally, a quaternary g-C_3N_4/Fe_3O_4/$CuWO_4$/CuO (CNFCC) heterojunction is generated by heating the final item for three hours at 500 °C. The g-C_3N_4/Fe_3O_4/$CuWO_4$ nanocomposite was not added when preparing solely CuO utilizing the same approach [38].

2.3. Catalyst characterization

The synthesized nanomaterial has been characterized via a several methods, which include energy-dispersive X-ray spectroscopy ((EDX) Ultra55, ZEISS), scanning electron microscopy ((SEM) Ultra55, ZEISS), transmission electron microscopy (TEM) JEM2100F, JEOL, UV-vis diffuse reflection spectra (DRS) analysis on a SHIMADZU UV-2600 spectroscopy instrument (Germany), and X-ray diffraction (XRD, Bruker, D8, Cu-Kα radiation). Nicolet 5DX-FTIR spectra, Fourier transformation infrared spectrum (FTIR), and vibrating sample magnetization by (VSM-EZ7-Microsence, Japan). Nitrogen adsorption at 77 K was used to calculate the Brunauer-Emmett-Teller (BET) particular surface areas using a Micromeritics Gemini-2390 surface area analyser. The same device is used to calculate the average volume of pores (cm^3/g), the average pore diameter in nm, and the pore size distribution using the Barrett Joyner - Haldena (BJH) technique. analysis of photoluminescence (PL) via a Japanese Hitachi F-7000 spectrometry.

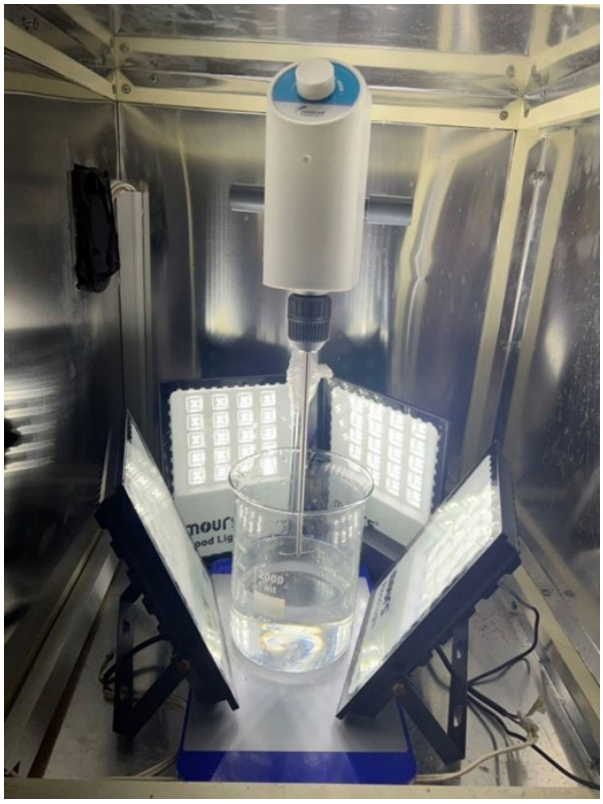

Figure 3. Setup of the batch photo reactor utilized for the photocatalytic process.

2.4. Photocatalytic Degradation Measurements

The chemical chlorpyrifos as a selected contaminant, the photocatalytic effectiveness of g-C_3N_4/Fe_3O_4/$CuWO_4$/CuO nanocomposites was evaluated when subjected to visible light. Four 50W LEDs were employed in a batch photoreactor for the standard studies (Figure 3) The LED lamps used in this experiment have a visible light wavelength range, which is normally between 400 and 800 nm. A set quantity of photocatalyst (1.5 g) was added to 1000 mL of CPF (10 mg/L) insecticide mixture for each run while being stirred using a mixer. To establish the adsorption equilibrium, the suspension was agitated for 30 minutes in darkness before getting exposed to visible light. Three milliliters of sample were gathered at 15-minute intervals for assessing photocatalytic activity, and a Shimadzu UV-2700 UV-Vis spectrophotometer was applied to identify each CPF's concentration at 290 nm of wavelength. In the presence of light, the control experiment was carried out without the use of a catalyst. The efficiency of photocatalytic degradation was obtained using the initial concentration of CPF (C_o) and its concentration throughout different irradiation times (C_t). The removal effectiveness (%) of CPF was measured using Equation (1) [39].

$$Removal\ Efficiency\ (\%) = \frac{(Co-Ct)}{Co} \times 100\% \qquad (1)$$

3. Results and Discussion

3.1. The Chemical Structure

In accordance with Figure 4A, the detected XRD pattern for CN is highly indexed with JCPDS No. 87-1526. Due to the unique interplanar stacking of the conjugated aromatic structure, the highest intensity peak 27.675 ^{o} is indexed as the (002) plane, while the largest peak at low intensity peak (2Θ) 13.825 ^{o} matches the (001) diffraction plane [40]. Three higher intensity peaks of 23.825 ^{o}, 30.475 ^{o}, and 36.425 ^{o} for quaternary g-C_3N_4/Fe_3O_4/$CuWO_4$/CuO nanocomposites demonstrate that the original crystal structure of g-C_3N_4 remains unchanged following the addition of Fe_3O_4 ,CuO and $CuWO_4$ nanoparticles to the outer layer of CN [41,34]. The XRD patterns show varying degrees of crystallinity. The CN sample shows a huge, amorphous-like peak around 2θ = 27° (black line), indicating a poor degree of long-range

ordering. When (CNFCC) sample differ with 2θ = 23.825°, 30.475°, and 36.425°, higher crystallinity is indicated by sharper, more prominent peaks. Higher ordering often leads to greater mechanical strength and stability compared to amorphous materials, but it can also reduce flexibility or reactivity. Variations in peak brightness among the sample suggest differences in the particle size distribution [34].

The variation in the functional groups during the synthetic procedure was examined using the FT-IR spectrum as seen in Figure 4B. Furthermore, the typical bending modes of CN heterocycles and C-N from g-C_3N_4 have been attributed to the major absorbance bands at 3239 cm^{-1} and 806 cm^{-1}. Three quite noticeable extra peaks can be detected in the Z-scheme g-C_3N_4/Fe_3O_4/$CuWO_4$/CuO heterojunctions' FT-IR spectrum at 562 cm^{-1}, 1648 cm^{-1}, and 2170 cm^{-1}. Based on these findings, g-C_3N_4, Fe_3O_4, $CuWO_4$ and CuO demonstrate a significant interaction; [42]. The most apparent change, especially at greater concentrations, is the expansion of the peak at 2170 cm^{-1}, which corresponds to C-N vibrations caused by stretching in the g-C_3N_4 framework in the CNFCC heterostructure [43]. The highest point 2170 cm^{-1} close to corresponds to the stretching vibration of the terminal nitrile (–C≡N) or cyano group, resulting from partial degradation or alteration of the g-C_3N_4 structure, area in 2100-2200 cm^{-1} composites is typically attributed to nitrile species (–C≡N), which are created when the triazine ring or terminal (–N=C=S) bonds as opposed to the typical stretching of amines and amides [44].

3.2. Morphological Properties

The collected samples' shape, content, and size of particles were investigated by SEM [45]. Figure 5A clearly demonstrates a sheet of gray g-C_3N_4 nanocomposites, whereas Figure 5B illustrates that the pristine $CuWO_4$ consists of uniform nanoparticles with a specific agglomeration, alongside a median particle dimension of fewer than 100 nm [9]. It is apparent from the SEM image shown in CuO Figure 5C that the CuO nanoparticles were irregularly circular crystalline particles with a mean length ranging from 34.17-60.51 nm [46,47]. In CNFCC, Fe_3O_4 ,$CuWO_4$ and CuO fragments are heavily deposited upon the outermost layer of the multilayered CN sheet in the shape of irregular flowers that appear to be stone-like microscopic crystals to form CNFC nanocomposites as shown in Figure 5D [48]. In the CNFCC TEM picture, g-C_3N_4 can be recognized by its bright gray hue with a thin film thicknesses. The Fe_3O_4 nanoparticles are recognized as having big, dark sphere-shaped particles, while both CuO and $CuWO_4$ floral architectures appear in black in Figure 5E ,The creation of a strong, porous, and tight CNFCC heterojunction architecture intended to maximize charge separation and enhance active sites, resulting in effective photocatalytic degradation of chlorpyrifos, is thus confirmed by the combined SEM/TEM results.

Figure 6(A) and (B) demonstrate clearly the composite's amazing crystalline structure. The EDS analysis revealed the composition of the g-C_3N_4/Fe_3O_4/$CuWO_4$/CuO hybrid consisted of Cu, W, Co, O, Fe, N, and C elements. This demonstrates an excellent distribution of elements throughout the CNFCC composite, reflecting a uniform immobilizing of nano-species over CN sheets, and this confirmed that a perfect heterojunction was attained among the nano particles in CNFCC heterostructure. Figure 6 (C–I) shows extra chemical and elemental characterization of the created photocatalysts through EDX and elemental mapping techniques.

The structural characteristics of the g-C_3N_4/Fe_3O_4/$CuWO_4$/CuO nanocomposite were

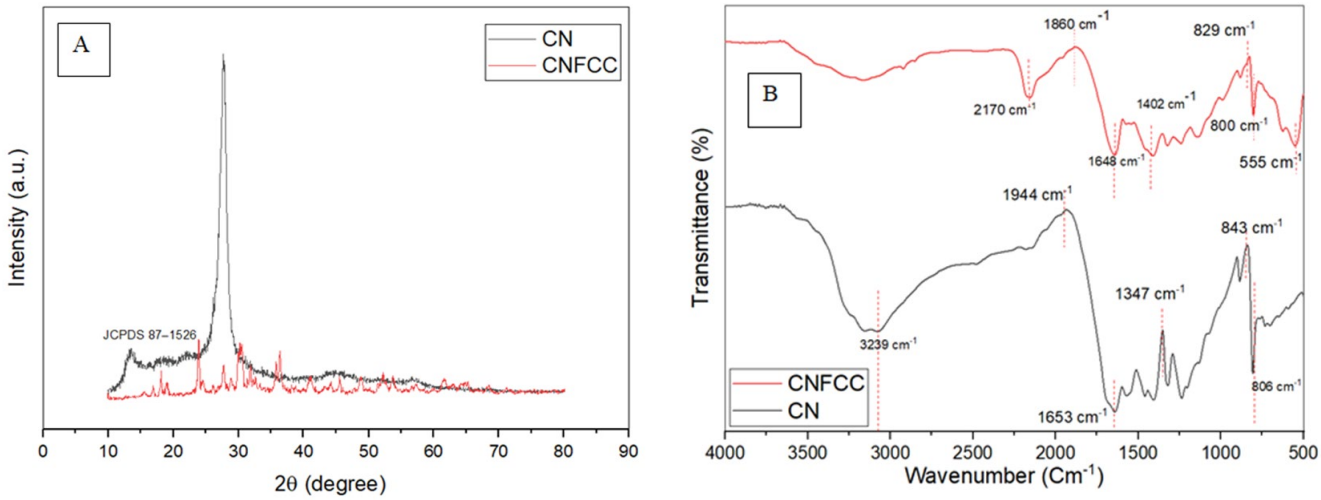

Figure 4. (A) XRD layouts of g-C_3N_4 and CNFCC, (B) FTIR spectrum of g-C_3N_4 and CNFCC.

studied using force microscopy (AFM) (Figure 6 J and K). The presence of unstructured sheet-like g-C_3N_4 nanostructures with an average height of less than 13.92 nm was verified by the results of 2D and 3D AFM pictures. Furthermore, the AFM images revealed that $CuWO_4$, CuO, and Fe_3O_4 nanoparticles were properly deposited on g-C_3N_4 nanosheets, enhancing the surface characteristics of the quaternary heterojunction , These outcomes also agreed with the results of the TEM and SEM.

BET and BEJ investigations were carried out to assess the specific surface area (S_{BET}), volume of pore, and diameter of the pores for both pure g-C_3N_4 and g-C_3N_4/Fe_3O_4/$CuWO_4$/CuO. The freshly prepared catalysts' nitrogen adsorption–desorption isotherms and distributions of pore sizes are displayed in Figure 7A and B. The surface areas, pore volumes, and diameters of pore for CN and CNFCC catalysts' were 8.844 m^2/g, 0.1458 cm^3/g, and 29.581 nm, and 25.4995 m^2/g, 0.170323 cm^3/g, and 51.149 nm respectively. These bigger surface areas in CNFCC represent a higher percentage of active sites, resulting in improved the photocatalytic efficiency [49].

3.3. Photoelectrochemical and Optical Analytics

UV-vis DRS was applied to investigate the photocatalysts CN, $CuWO_4$, CuO and CNFCC's absorption of light capabilities. The

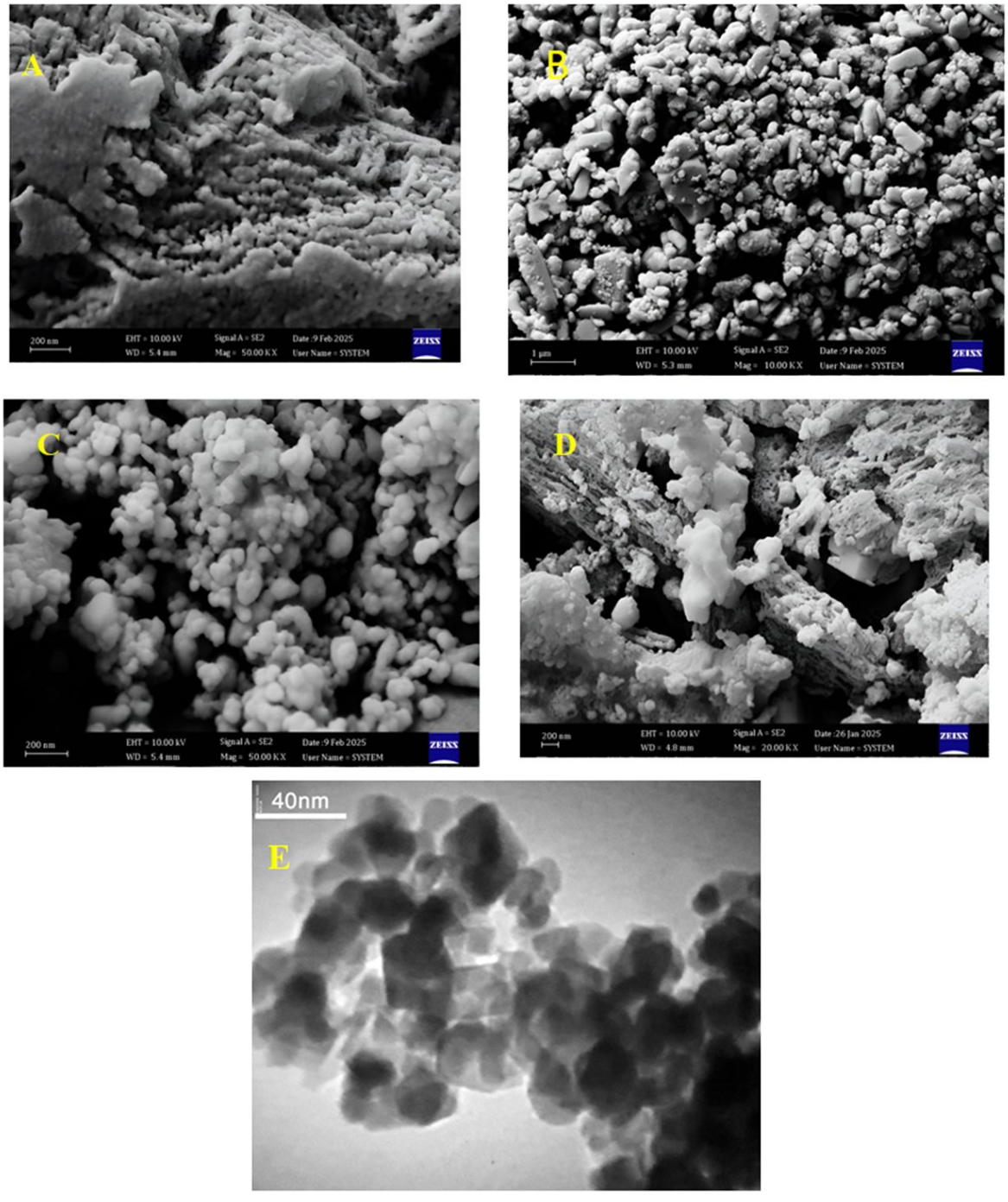

Figure 5. SEM images of (A) pristine CN, (B) CuO, (C) $CuWO_4$, (D) CNFCC, (E) TEM image of CNFCC.

heterojunction's generation enlarged the photocatalyst's absorption edge, thus potentially improving its photocatalytic effectiveness. The bare CN nanosheet and $CuWO_4$ tiny flakes revealed a narrow absorption edge of less than 450 and 500 nm, accordingly [25]. Figure 8A The phase diagram (PL) spectra of pure g-C_3N_4, $CuWO_4$, CuO, and CNF, CNFC, CNFCC compound are presented. For CuO, the excitation wavelength is 400 nm in wavelength. For the pure form of g-C_3N_4, the main emission peak lies at approximately 438 nm. This finding indicates that individual systems may achieve an excellent recombination rate while sacrificing charge transfer performance [49]. In addition, compared to the pure form of g-C_3N_4, CNFCC exhibits noticeably lower emission peak intensities, suggesting a reduced rate of electron–hole recombination. It could be explained by the firm heterostructures that are among CNFC and CuO, which enable the transfer of electrons as well as holes. afterwards CuO connecting on the g-C_3N_4 surface, the PL intensity strongly falls in due to of CuO's and $CuWO_4$ effective carrier charge separation, which minimizes the rate of recombination of e^-/h^+ pairs. In overall, a higher

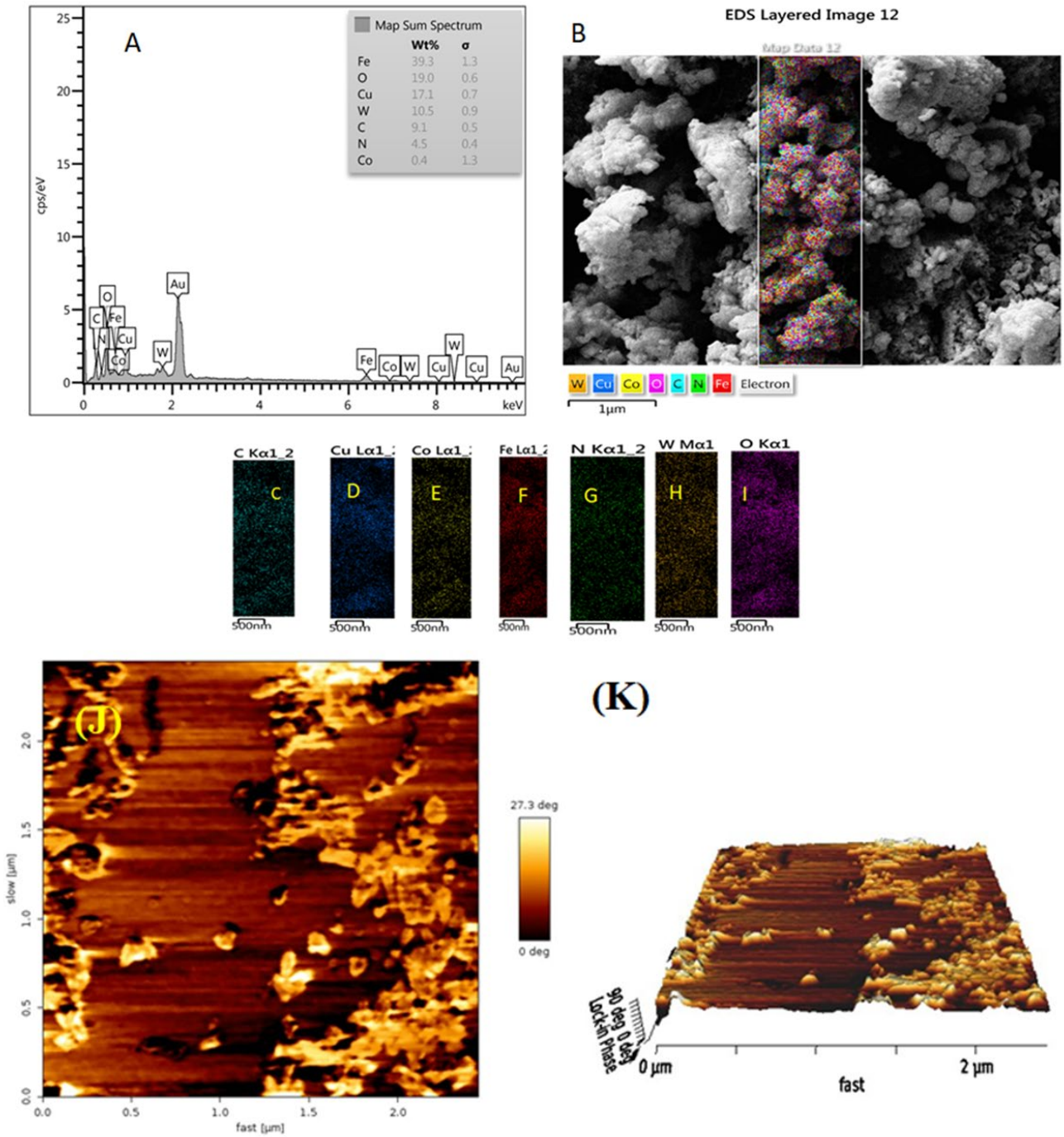

Figure 6. (A) and (B) EDX spectrum CNFC composites. EDX analysis ,(C–I) elemental mapping of C, Co, O, Cu, Fe, N, O, and W elements; (J) 2D AFM imaging of the CNFCC compound, (K) 3D AFM imaging of the CNFCC compound.

separation effectiveness for photogenerated carriers is associated with a decreased emission of PL signal [39]. The absorption spectroscopy approach is used to determine the optical characteristics of the materials that are generated by Uv-vis DRS analysis (CN, $CuWO_4$, CNF, CNFC, and CNFCC), as shown in Figure 8 B. This technique offers crucial information about the

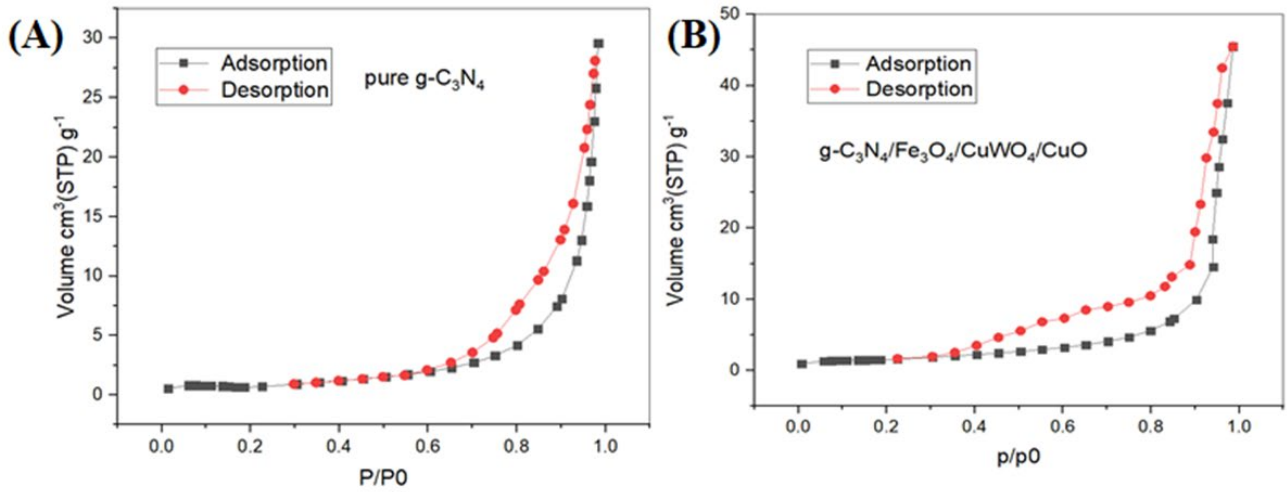

Figure 7. N_2 adsorption–desorption isotherms for (A) pristine CN and (B) CNFCC nanocomposites.

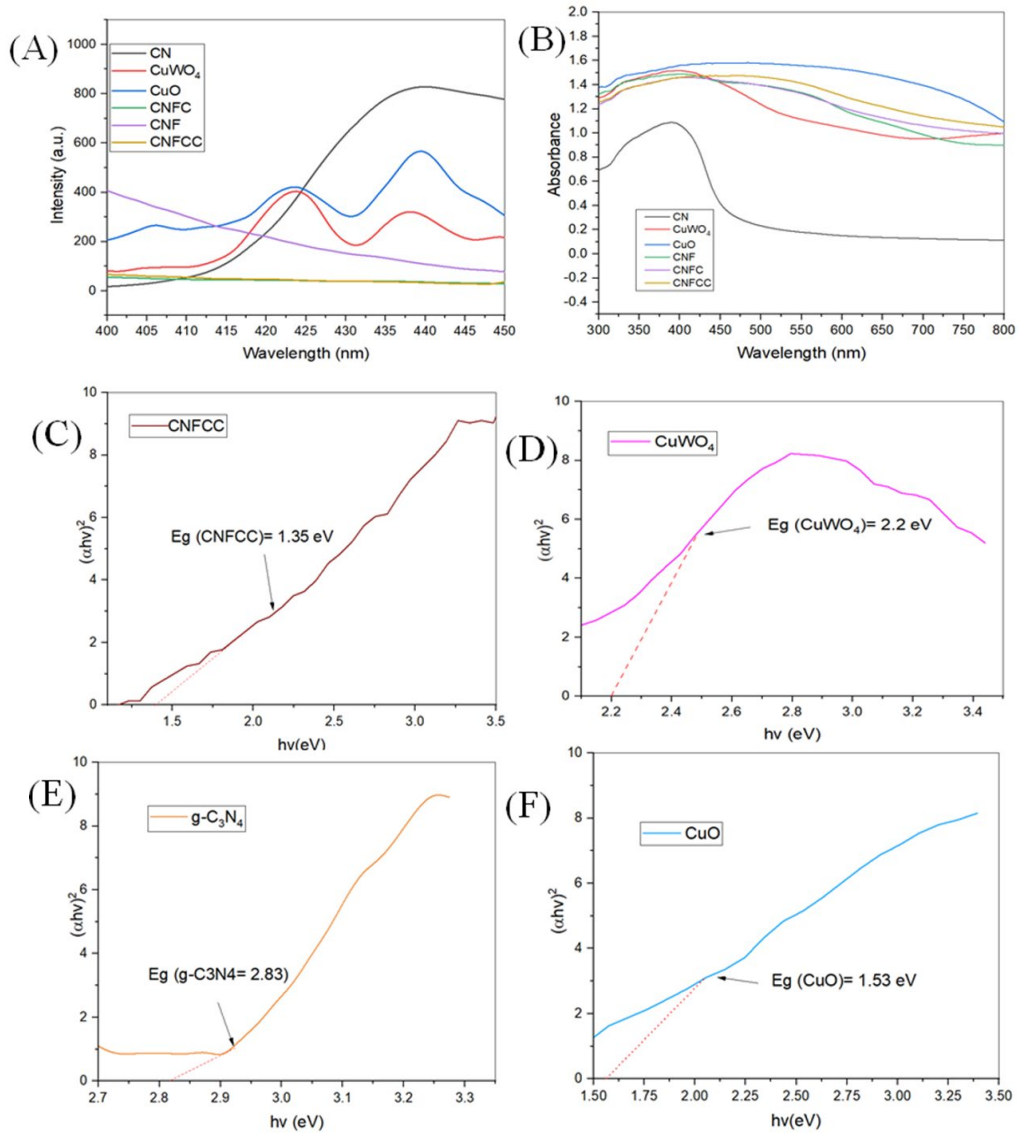

Figure 8. (A) PL spectra of pure CN, $CuWO_4$, CuO, CNF, CNFC, and CNFCC composite. (B) The DRS spectra of photocatalysts and (C), (D), (E) and (F) Plots of $(ahv)^2$ against (hv) for CNFCC and pristine CN, $CuWO_4$, CuO.

absorption of light by the heterogeneous photocatalysts [15]. The bare CN nanosheet and CuWO4 nanoflakes have been revealed to have tight absorption limits of less than 450 and 500 nm, respectively. It also suggests that ultraviolet light can be absorbed by the bare g-C_3N_4 and $CuWO_4$ semiconductors [34]. The absorption edge for CNFC was evidently extended to 750 nm after $CuWO_4$ was applied to the nanocomposite materials. The CNFCC composite's optical qualities were substantially improved by applying light at the visible limits (400–800 nm).

The outcomes of UV-Vis can be visualized by extrapolation the linear part of the plot to the hυ axes, and the estimated bandgap energy was calculated using Tauc's connection equation Equation (2). The band gap of each sample was next verified using the Tauc plot; for $CuWO_4$, pristine CN and CuO the bandgap energy was 2.2 eV ,2.83 eV and 1.53 eV, subsequently, as illustrated in Figures 8 C -F.

$$(ahv)^{1/n} = C \times (hv - E_g) \quad (2)$$

where n = ½ and 2 for both direct and indirect band gaps, accordingly, and hv is the incident energy of the photon, C is the constant for proportionality, and the band gap energy is indicated by E_g [51].

3.4. The Magnetic Properties

The CNFCC photocatalyst's magnetic features have been demonstrated via the VSM experiment. The hysteresis curve in Figure 9 reflects the vibrating sample magnetometer (VSM) data. For CNFCC and CNF, the predicted values for the saturation magnetization (Ms) were 13.041 and 14.11 emu/g, respectively. The magnetic attraction of Fe_3O_4 nanoparticles was verified by this finding, which proved that the produced CNF nanocomposite had the highest Ms value [52]. The existence of non-magnetic $CuWO_4$ and CuO nanoparticles inside the CNFCC nanocomposite is another variable attributing to this drop in MS measurement. The consequent nanocomposite sustains a substantial magnetic power despite a decline in magnetic values, thus enabling efficient magnetic remembrance of the nanocomposite following multiple running cycles [49]. Low loss of energy during magnetization processing had been demonstrated by the hysteresis loop's configuration, which made the nanocomposite perfect for magnetic separation and targeting [53,54].

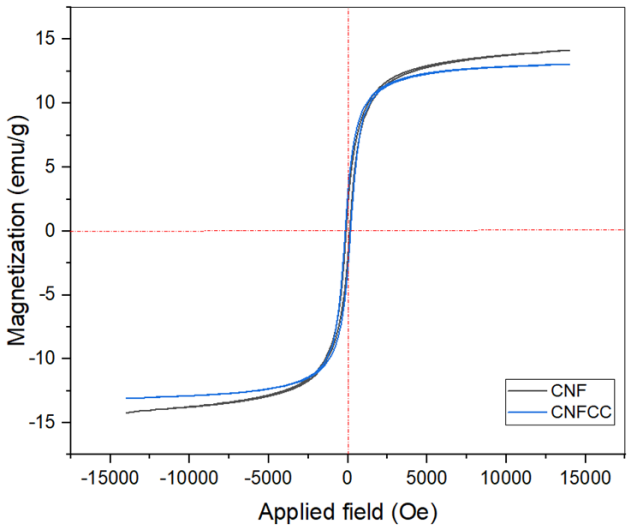

Figure 9. Magnetic properties of CNF and CNFCC.

3.5. Adsorption and Photodegradation Activities

In order to assess the activities of manufactured catalysts, the photodegradation of a CPF aqueous solution (10 mg/L, pH of 5, catalyst dose 1.5 g/L) under LED irradiance was performed. As a result, a blank experiment employing the CPF solution without any photocatalyst had been carried out. No noticeable CPF deterioration was observed during 150 minutes of irradiation without a photocatalyst. The adsorption and photodegradation properties of synthetic catalysts' (CN, $CuWO_4$, CuO, CNF, CNFC, CNFCC) towards CPF as a representative organic pollutant undervisible light illumination for 150 min. Without photocatalysis, CPF demonstrated a very low rate of degradation; following 150 minutes, no apparent degradation was observed, indicating that CPF's natural breakdown can be disregarded.remarkably, after 30 minutes of adsorption in darkness control, the bare CN exhibited the lowest adsorption performance of 12% against CPF. Based to the BET data, pure g-C_3N_4's restricted adsorption activity was explained by its lesser surface area.Additionally, at 30 minutes, CPF's adsorption performance for $CuWO_4$ and CuO was 20% and 23%, respectively. Further, when compared to bare CN, the absorption effectiveness of the binary CNF nanocomposite and ternary CNFC enhanced simultaneously, by 15% and 26% for CPF.When compared to bare CN nanosheets, binary, and ternary composites, the quaternary CNFCC composite displayed increased adsorption performance, eliminating 33% of the CPF in 30 minutes. This can be explained through the fact that CuO helps strengthen the surface structure of the CNFCC composite, which exposes more active sites to increase photocatalytic activity. At 120 minutes of LED irridation, the proportions of pure CN, CNF, CNFC, $CuWO_4$, and CuO degradation were 41%, 45%, 60%, 75%, 58%, and 53% for CPF, accordingly. These outcomes were caused by the elevated recombination rate of bare CuO and the lower visible light usage abilities of immaculate CN and $CuWO_4$. Due to the enhanced

hetrojunction between the CN and $CuWO_4$ semiconductors, the g-C_3N_4/Fe_3O_4/$CuWO_4$ composites demonstrated an 88% rate of degradation for CPF at 135 minutes.nevertheless, in contrast to the other compounds, the quaternary g-C_3N_4/Fe_3O_4/$CuWO_4$/CuO showed the best photocatalytic effectiveness, with a degradation rate of 93% at 150 minutes for CPF of LED irrigation. This is due to the adsorption activity and visible light absorption ability of the g-C_3N_4/Fe_3O_4/$CuWO_4$/CuO were substantially improved following the depositing of CuO, which increased the surface area of the CNFCC composite and active sites, as measured by the BET analysis (Figure 10A). The degradation constant of g-C_3N_4/Fe_3O_4/$CuWO_4$/CuO has been determined to be stronger than that of the samples created from CN and $CuWO_4$, indicating that CNFCC's photodegradation performance has been significantly enhanced.

At 150 minutes under LED exposure to light, the efficiency elimination of TOC and COD of CPF in aqueous solution were 58% and 69 %, consequently (Figure 10 B). This indicates that an important amount of CPF molecules that were destroyed by strong oxides, such as $^{\cdot}OH$, $^{\cdot}O_2^-$, and h^+ radicals, were actually converted to CO_2 and H_2O in presence of CNFCC nanocomposite. Furthermore, the breakdown of organic matter caused the formation of intermediate products, which diminished the removal of COD and TOC [55].

3.6. Kinetic Studies

The kinetics of the photocatalytic reaction have been investigated utilizing the Langmuir–Hinshelwood kinetic model [19,32]. The representation of pseudo- first-order kinetics is offered by Equation (3).

$$\ln \frac{C}{C_\circ} = kt \quad (3)$$

where k is the rate constant, C_0 is the initial concentration, and C_t is the concentration at time t. [56]. Table 2 demonstrates gradient of the plot -

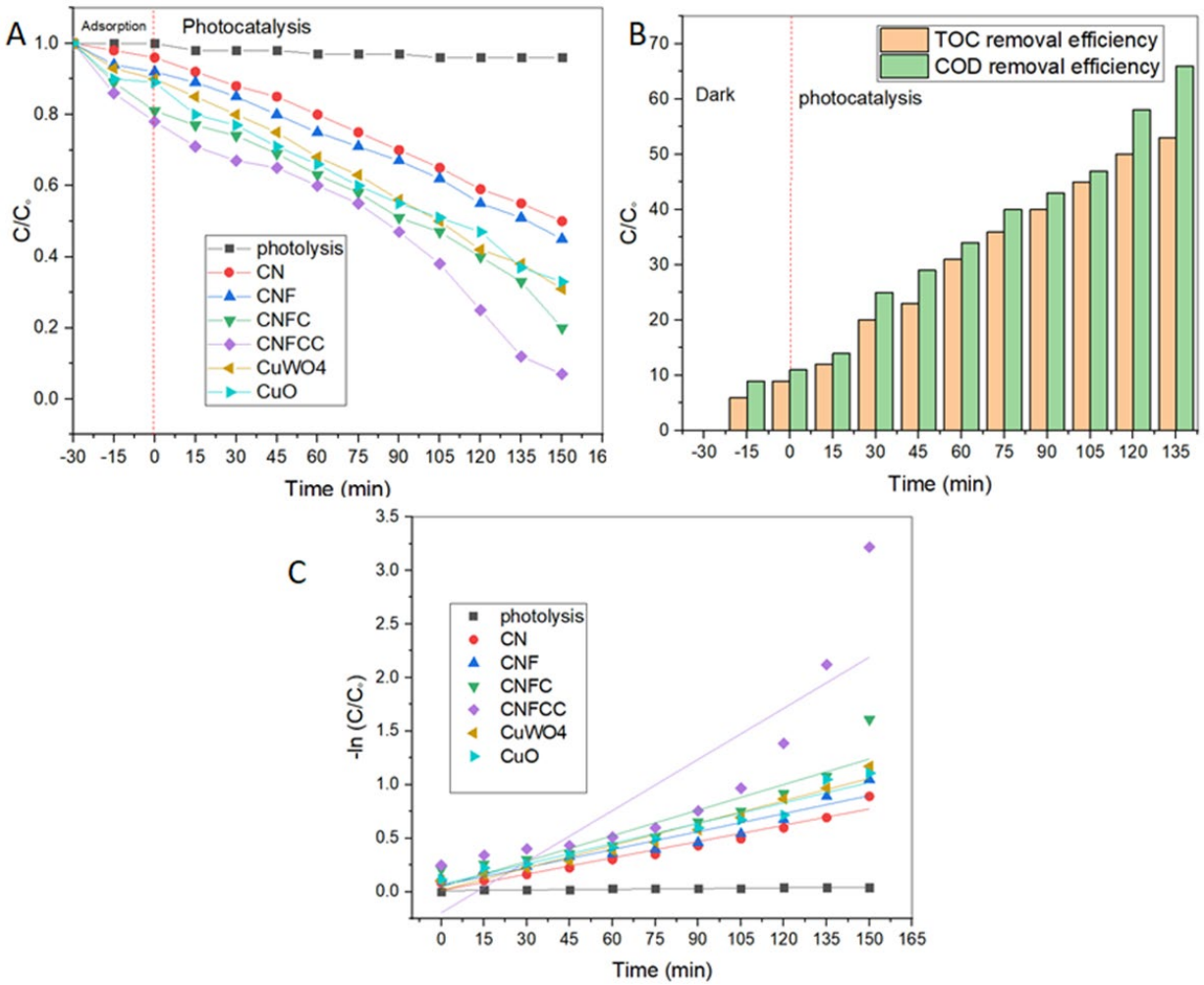

Figure 10. (A) Efficiency of removal for CPF using visible light for the catalysts (CN, CNF, CNFC, $CuWO_4$, CuO, and CNFCC) under catalyst dosage = 1.5 g/L and t = 150 min, (B) The as-fabricated photocatalyst's first-order kinetics approaching CPF while exposed to visible light, (C) CPF's mineralization efficacy for TOC and COD.

ln (C/C_0) vs. t (min), comprised the estimated k values. As seen in Figure 10 C, the findings from the experiment exhibited an excellent coefficient of regression (R^2) and matched pseudo- first-order kinetics (Equation (3)) exactly.

3.7. Operating Conditions Effects

3.7.1. Effect of CNFCC dose

A series of tests were carried out to determine the appropriate catalyst loading through adjusting the quantity of the best photocatalyst in order to prevent an excess of catalyst and ensure complete absorption of efficient photons [57]. The photodegradation rate of CPF was researched using varying dosages of the g-C_3N_4/Fe_3O_4/$CuWO_4$/CuO photocatalyst (0.5, 0.75, 1, 1.5, and 2 g/L). The experiments' data, which are shown in Figure 11A, indicate that CPF photodegradation performances increased progressively as the dosage of g-C_3N_4/Fe_3O_4/$CuWO_4$/CuO rose up to 2 g/L. According to [58,59], raising the catalyst mass suggests to increase the number of hydroxyl

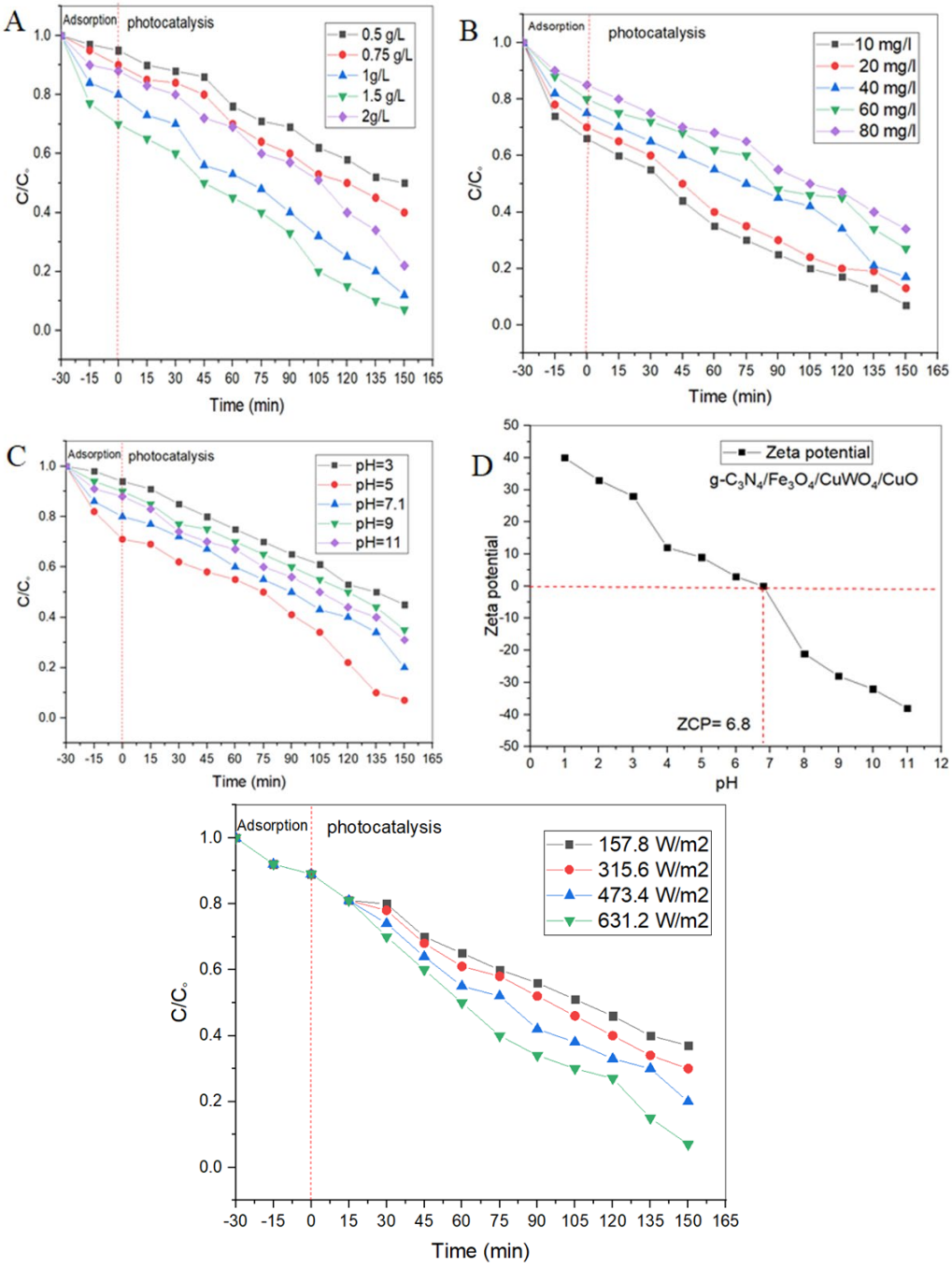

Figure 11. Operational conditions' impacts on CNFCC photodegradation toward CPF: (A) Effect of CNFCC dosage; (B) Effect of CPF concentration; (C) The impact of solution pH; (D) Zeta potential assessment with PZC estimation, (E) impact of light intensity.

radicals via raising the total amount of absorbed photons (high density of molecules in the area of illumination) as well as adsorbed contaminant molecules. As exposed to LED light for 150 minutes, the removal effectiveness of CPF over catalytic dosages of 0.5 and 0.75 g/L were 50% and 60%, correspondingly, but at 2 g/L, they were 66% and 78% for CPF at 120 and 150 minutes of irradiation time. Additionally, the effectiveness of the active sites creating free radicals dropped as the number of catalysts raised beyond 2 g/L since light absorption reduced. The catalyst loading of 1.5 g/L is more beneficial in terms of photocatalytic effectiveness based on the earlier information because a higher Removal efficiencies of CPF were observed at this dose, which was 93%. The high Specific Surface Area and Total Pore Volume found in the BET analysis for CNFCC are directly responsible for the degradation rate's linear rise to dosage (1.5 g/L). For the production of reactive oxygen species (ROS), these structural characteristics offer a high density of accessible active sites. However, "light shielding," in which the extra particles (shown as spherical clusters in SEM/TEM pictures) raise the turbidity of the solution and prevent photon penetration to the catalyst, is responsible for the observed decrease in efficiency beyond the optimum dose [7].

3.7.2. Effect of CPF concentration

Higher concentrations cause lower photooxidation rates due to fewer reactive species have the ability to attack the pollutant molecules as concentration increased [60]. As shown in Figure 11B, the degradation performance of the CPF was 83%, 80%, 66%, 55%, and 53% during 120 minutes of LED irradiation. The degradation efficiency was estimated using multiple concentrations of CPF (10, 20, 40, 60, and 80 mg/L) employing 1.5 g/L of g-C_3N_4/Fe_3O_4/$CuWO_4$/CuO. At 150 minutes, CPF's degradation performance under LED irradiation was 93%. It could be connected with a reduction in photogenerated hydroxyl radicals and positive holes, in addition to the increase of CPF molecules inhabiting the photocatalyst's active sites [61]. The follow-up experiment's CPF concentration of 10 mg/L was selected because there were many active sites on the catalytic surfaces for CPF molecules at that concentration. On the other hand, CPF molecules inhibited the nanocatalyst from absorbing light at larger concentrations (20 mg/L or more than 20 mg/L), which reduced hydroxyl radical generation and, as a result, the breakdown of the desired pollutant [62,63]. As the concentration of chlorpyrifos rose, a decrease in the degradation efficiency was noted. The saturated state of the accessible active sites, which is shown by a BET surface area, can account for this. The mesoporous structure of the catalyst permits effective diffusion at lower concentrations, but at larger levels, the pollutant molecules "shield" the catalytic surface, according to the BJH pore size distribution. This "UV-screening effect" lowers the production of reactive radicals by blocking photons from accessing the active sites found in SEM/TEM investigation [6].

3.7.3. Effect of pH

The pH of a solution has an important function in regulating the charged species of contaminant molecules, and the charges that accumulate on the catalyst's surface additionally have an impact on the factors which affect the photodegradation process's performance [64]. As shown in Figure 11C, the influence of solution pH on CPF photodegradation (10 mg/L) was examined using 1.5 g/L of g-C_3N_4/Fe_3O_4/$CuWO_4$/CuO photocatalyst at various pH levels (3, 5, 7.1, 9, 11).

In accordance with Figure 11 D, the CNFCC's pH_{pzc} (pH value for zero-point charge) was 6.8. Therefore, when the pH is lower than 6.8, the quaternary CNFCC exhibits a positive surface Because both PCF and the catalyst have a positive charge at pH of 3, an electrostatic repulsion will develop between CPF molecules and the catalyst surface, reducing the effectiveness of adsorption and degradation. Because the CPF molecules' positive charge endures while the CNFCC changes to a negative charge, an electrostatic attraction develops between the PCF molecules and the catalyst surface in (pH between 5 and 7.1), increasing adsorption and photocatalytic efficiency [6,65]. Ultimately, Low adsorption and photodegradation efficiency results from

Table 2. The results of first order kinetics for the breakdown of CPF using different photocatalysts.

Photocatalyst	k (min^{-1})	R^2
Photolysis	2.1818×10^{-4}	0.83077
g-C_3N_4	0.00507	0.96043
$CuWO_4$	0.00696	0.96839
CuO	0.006886	0.95109
g-C_3N_4/Fe_3O_4	0.0056	0.91912
g-C_3N_4/Fe_3O_4/$CuWO_4$	0.00796	0.86798
g-C_3N_4/Fe_3O_4/$CuWO_4$/CuO	0.0159	0.85963

electrostatic attraction between CPF molecules and the catalyst surface because both CPF and the catalyst are negatively charged (pH greater than 7.1) [66]. PZC estimation utilizing zeta potential analysis was shown in Figure 11 D. After 150 minutes of LED irradiation, it was obvious that CPF photodegradation was strong at pH values of 5 , which were close to the ZCP value. The elimination rate of CPF was 93% and 80%, respectively. According to this study, the ideal pH level for CPF elimination via CNFCC heterojunction was found to be 5. Surface charge or zeta potential, as determined by characterization, is a governing factor in the photocatalytic degradation of CPF from aqueous solution, as seen by the decrease in degradation at higher pH being attributed to electrostatic repulsion.

3.7.4. Effect of light intensity

Because it directly influences the creation of active hydroxyl radicals, the intensity of light is an essential variable in the photocatalytic degradation reaction. The intensity of the irradiated light controls the generation of electron and hole pairs in semiconductors [67]. Over g-C_3N_4/Fe_3O_4/$CuWO_4$/CuO nanocomposite (1.5 g/L), the effects of the intensity of light (157.8 W/m^2, 315.6 W/m^2, 473.4 W/m^2, and 631.2 W/m^2) on the photo-destruction of CPF (10 mg/L) were investigated. As demonstrated in Figure 11 E, the photo-oxidization effectiveness of CPF was clearly weakened when the light intensity dropped from 631.2 W/m^2 to 157.8 W/m^2. At 150 minutes of LED exposure, photodegradation activity for CPF reached 93% for 631.2 W/m^2, while photodegradation activity was 63% for light intensity 157.8 W/m^2 at the same time. The main reason of this discovery, which had been demonstrated in earlier investigations, was that increased intensity of light enhanced the photolytic reaction ratio, generated more photons in a specific period of time, and enabled an increased degradation yield [68]. The UV-Vis DRS analysis, which revealed a narrow band gap for CNFCC of [1.35 eV], directly supports the results, which demonstrated a linear rise in efficiency with greater intensity 631.2 W/m^2. Effective photon absorption is made possible by this narrow band gap. Additionally, the low-intensity peaks in photoluminescence (PL) spectra, which show a suppressed recombination of photo-generated electrons (e^-) and holes (h^+), are consistent with the high degradation rate even at moderate intensities, allowing a greater number of charge reach the catalyst surface for pollutant degradation. The low PL intensity indicates that these charges are effectively separated rather than recombining, whereas the linear increase in rate constant with light intensity shows efficient creation of electron-hole pairs [34,52].

3.8. Recyclability of the as Created Photocatalyst

The reusability of the nanocomposites has been investigated via six successive cycles at ideal operating conditions, as depicted in Figure 12 A. Following the six cycles of operation, the photoactivity of g-C_3N_4/Fe_3O_4/$CuWO_4$/CuO revealed a slight decline from 93% to 77%. Some substance loss and perhaps partial inactivation of active sites might be the reason of this gradual decline. Nonetheless, the generated CNFCC nanocompsoites' photocatalytic activity stayed consistent [40,53]. Most importantly, XRD, VSM, DRS, SEM, and TEM investigations verified that the composition and morphology of g-C_3N_4/Fe_3O_4/$CuWO_4$/CuO remained similar after the reaction, highlighting the absence of structural modifications (Figure 12 B-F).These results highlight CNFCC's outstanding prospects as a photocatalyst for a range of uses.

3.9. A Plausible Explanation for the Degradation of CPF

To identify the primary active species throughout the CPF degradation across the CNFC heterojunction, radical trapping experiments have been carried out. consequently, EDTA-2Na (1 mmol.L^{-1}) was employed as a h^+ trapping chemical, benzoquinone (BQ, 1 mmol L^{-1}) as an $\cdot O_2^-$ scavenging chemical, and IPA (1 mmol.L^{-1}) as an $\cdot$OH scavenging agent. Without contributing to the photoreaction, such scavengers are able to capture the photogenerated active species and enable the process keep going [34].

Controlled studies involving different trapping agents were carried out to hypothesize on the mechanism of photocatalytic breakdown. The addition of (IPA) to trap $\cdot$OH significantly reduced the rate of CPF degradation, illustrated in Figure 13A. However, the rate of degradation would be lowered when (BQ) was added to trap $\cdot O_2^-$. This suggests that photogenerated $\cdot$OH and $\cdot O_2^-$ radicals played an important part in the reaction system, while EDTA-2Na (h^+) performed a minor one [45]. The charge-transfer process orientation and the mechanism of photocatalytic action are being investigated by examining the precise band configurations, the valence band (VB), and the conduction band (CB) of g-C_3N_4, $CuWO_4$ and CuO. The E_g of virgin g-C_3N_4 ,pure $CuWO_4$ and CuO has been determined to be 2.83 eV 2.2 eV and 1.53 ev, respectively. The following formulas can be employed for determining the semiconductors' Conduction band energy (E_{CB}) and valence band energy (E_{VB}):

$E_{VB} = X - E_e + 0.5\ E_g$ (4)

$E_{CB} = VB - E_g$ (5)

$\chi(A^mB^nC^l) = \sqrt[m+n+l]{xA^m xB^n\ xC^l}$ (6)

The free electron energy (4.5 eV) towards the hydrogen level is symbolized by E_e, whereas X indicates the semiconductor electronegativity (C =

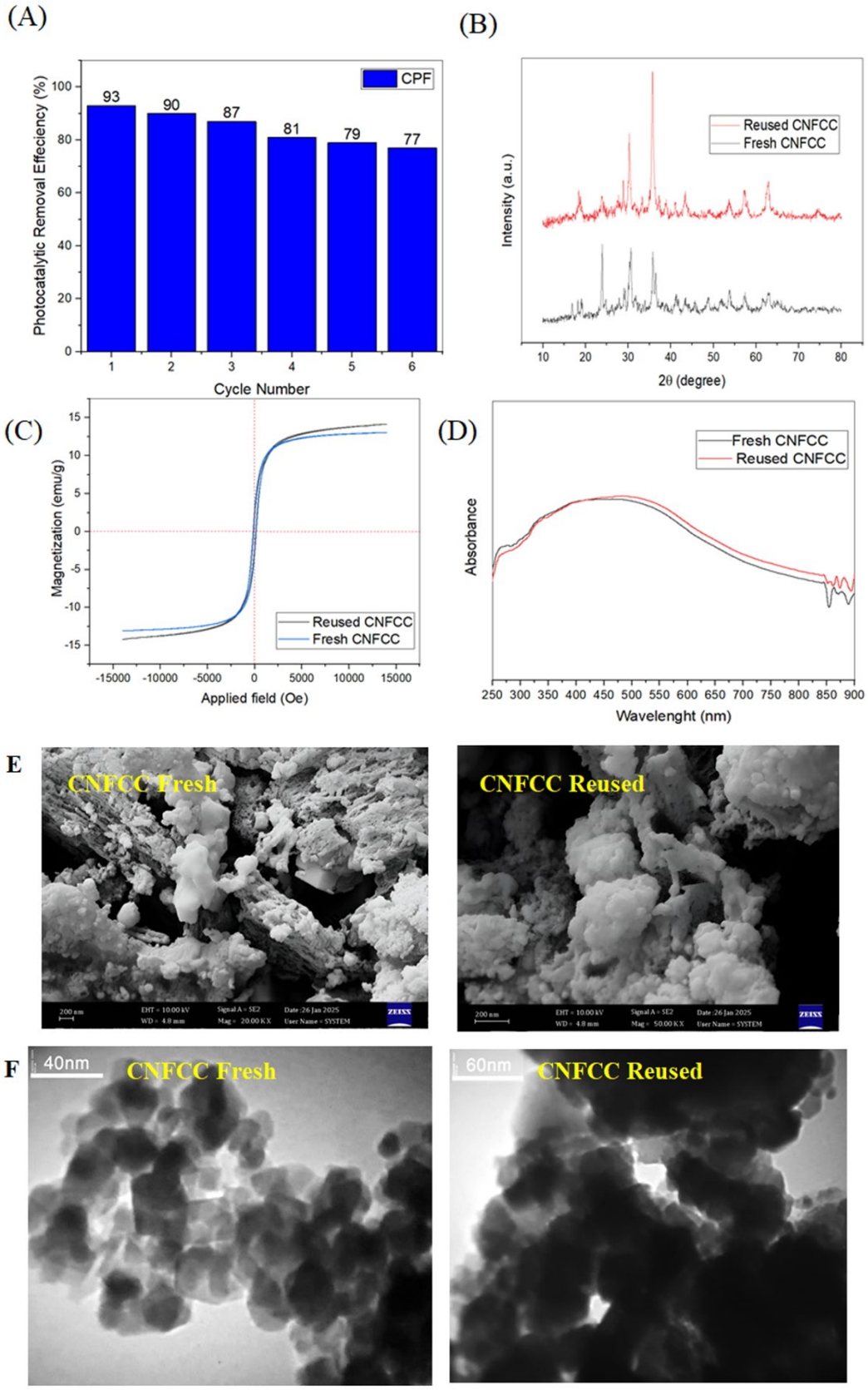

Figure 12. Evaluation of stability and reuse potential: (A) CPF degradation cycles at a running time of 150 min, CNFCC, Consistent 1.5 g/L catalyst dosage and 10 mg/L CPF concentration were maintained throughout all cycles. Characterization of photocatalysts prior to and following six cycles; (B) XRD patterns; (C) Hysteresis curves for VSM (D) DRS spectra; (E) SEM images; (F) TEM images.

6.27 eV, N = 7.3 eV, Cu = 4.48 eV, W = 4.4 eV, O = 7.54 eV) [69]. The VBs for g-C_3N_4, pure $CuWO_4$ and CuO are 1.57 eV, 2.9 eV and 2.31 eV, accordingly, according to these formulae (Equations (4-6)). Their CBs are -1.26 eV 0.7 eV and 0.78 eV. Further, the suggested Z-scheme degradation mechanism is illustrated in Figure 13 B. In this mechanism, electrons from the semiconductor with a greater negative charge CB can directly interact with VB from the opposite semiconductor to recombine with their holes, thereby generating a heterojunction that would aid in the photocatalytic process for CPF photodegradation [27,47].

The electrons in the quaternary heterojunction g-C_3N_4/Fe_3O_4/$CuWO_4$/CuO constituents excite from VB to CB when subjected to visible light, whereas the holes in the g-C_3N_4 and $CuWO_4$ remained in VB Equation (7). $CuWO_4$ displays the same phenomena, with electrons leaping to the conduction band and leaving the highly energetic hole in g-C_3N_4 behind. In VB of CN, the photogenerated holes would interact with the photogenerated electrons at the CB of $CuWO_4$,O_2 is successfully degraded to $^{\bullet}O_2^-$ by the photogenerated electrons in the CN conduction band (Equation (8)). The electrons produced by photolysis in the CuO CB travel and recombine with the holes that are formed in the VB of $CuWO_4$, and the photoinduced holes in the VB of g-C_3N_4 recombine with the electrons in the CB of $CuWO_4$ [18]. $CuWO_4$'s VB holes react with OH to produce.OH (Equation (9)). The organic pesticide is effectively broken down into a basic product by both $^{\bullet}O_2^-$ and $^{\bullet}OH$ (Equation (10)) [70]. The CPF may be oxidized to CO_2, H_2O, and other basic products by the radicals produced by light ($^{\bullet}OH$, $^{\bullet}O_2^-$, h^+, and H_2O_2) [71] in Equatiom (11).

$$CNFCC + h\upsilon \rightarrow (h^+ + e^-) \quad (7)$$

$$e^-\ (CB\ of\ g\text{-}C_3N_4) + O_2\ or\ H^+ \rightarrow (^{\bullet}O_2^- + H_2O_2)\ oxidants \quad (8)$$

$$(H_2O\ or\ OH) + h^+\ (VB\ of\ CuWO_4) \rightarrow {}^{\bullet}OH \quad (9)$$

$$H_2O_2\ or\ {}^{\bullet}O_2^- + e^- \rightarrow {}^{\bullet}OH \quad (10)$$

$$(h^+, {}^{\bullet}O_2^-, {}^{\bullet}OH, H_2O_2) + CPF \rightarrow CO_2 + H_2O + by\ product \quad (11)$$

3.10. Comparison versus Earlier Studies

Numerous studies regarding the photodegradation of CPF using various photocatalysts have been performed. Table 3, which includes background on the conditions of the experiment, contrasts the removal effectiveness identified for the CPF insecticides with those of prior studies.

4. Conclusions

The goal of this investigation is to boost the CNFCC nanocomposite's photocatalytic activity as a novel magnetic reusable photocatalyst. It is securely attached to the both $CuWO_4$ and CuO semiconductors and properly incorporated. Using visible light, the multi-step formed g-C_3N_4/Fe_3O_4/$CuWO_4$/CuO photocatalysts exhibited significantly more activity in breaking down CPF pesticide. Following 150 minutes of LED illumination, the degradation rate for g-C_3N_4/Fe_3O_4/$CuWO_4$/CuO approached 93% with rate constants (k) of 0.0159 min^{-1}. The g-C_3N_4/Fe_3O_4/$CuWO_4$/CuO heterostructure showed excellent optical and electrochemical characteristics that could boost the visible light

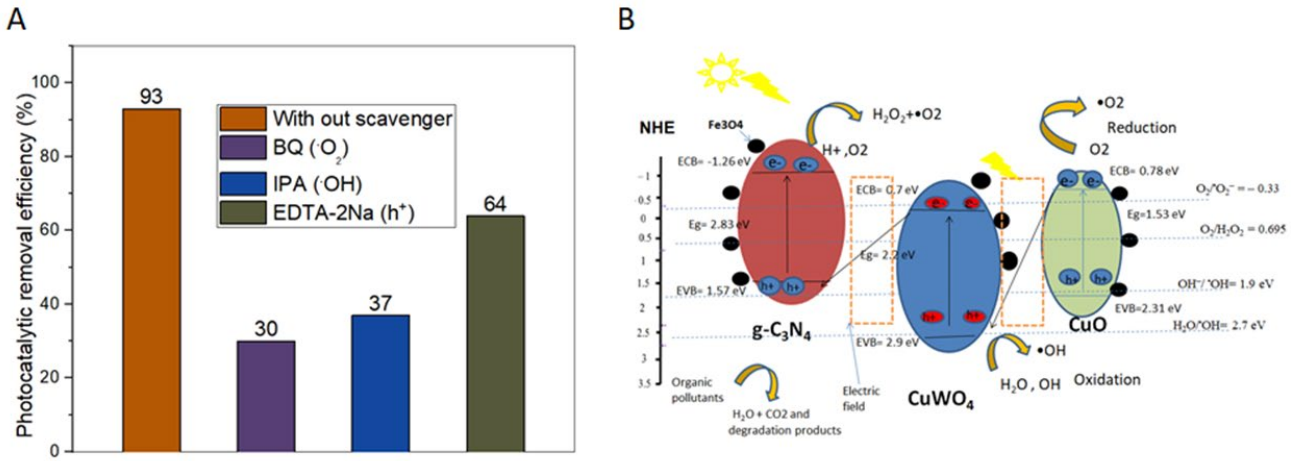

Figure 13. (A) Details of the CPF photocatalytic reaction trapping investigation, (B) CNFCC nanocomposite-based photocatalytic degradation procedure for CPF.

absorption spectrum. The efficiency elimination of TOC and COD of CPF in aqueous solution were 58% and 69%, consequently. The CNFCC heterojunction is remarkably stable, according to stability and reusability tests, and the formation of Fe_3O_4 on the surface of CN nanosheets significantly aided in obtaining adequate magnetic stability with an easy separable method. Tests of reusability proved the robustness and recyclable nature of the composites With a photodegradation efficiency of 77% after sixth cycle, the synthetic composite exhibited excellent reusability. ·OH is the primary active oxidant and h^+ contributes the least to the CPF reaction, according to the results and traps. Finally, scavenger studies confirmed the CNFCC nanocomposite's likely mechanism of CPF degradation, which was explained by Z-scheme pathways.Electron-hole pair interaction is lowered by the Z-scheme heterojunction configuration. The production of visible light-activated photocatalysts for the purification of wastewater and further investigations into pesticide breakdown pathways are made possible via these discoveries.

Acknowledgment

The authors declare that no funds, grants, or other support were received during the preparation of this manuscript.

CRedit Author Statement

Author Contributions: Shno M. Ali: Writing – original draft, Methodology, Data curation. Abeer I. Alwared: Writing – review & editing, Supervision, Project administration. All authors have read and agreed to the published version of the manuscript.

Table 3. Comparing the outcomes of present research regarding the photodegradation of CPF pesticides with the findings from past investigations.

Catalyst	Catalyst dosage (g)	Pollutant solution (mg/L)	Light source	Photocatalytic Applications	Method of synthesis	Ref.
$Zn_{0.5}/Ag_{0.5}/S$	0.03	100	UV lights (Xe-lamps, 300 W)	95% at 60 min	hydrothermal method	[72]
Fe/CeO_2-SiO_2	0.007	50	UV radiations	81.31%	hydrothermal method	[73]
Mn-WO_3/SnS_2	0.1	1	300 W xenon lamp	100% at 90 min	hydrothermal method	[7]
Fe_3O_4 and WS_2 nanoparticles on silica	0.05	7.2	300 W LED lamp	91% at 52 min	Multi steps mehod	[74]
S-Doped Ni–Co LDH/Fe_3O_4	0.06	2.5	LED lamp (50 W)	92.5% at 150 min	Multi steps mehod	[75]
CuO/TiO_2/PANI	0.045	5	300 W tungsten lamp	95% at 90 min	chemical reduction method	[61]
mZnO/TiO_2-Fe_3O_4	0.06	10	Visible light	94.8% at 100min	Multi steps method	[5]
ZnO@CdS	0.025	2	sunlight	91% at 360 min	green methodology	[76]
Cu-doped TiO_2/GO	0.3	100	UV and visible light	91.4% at 80 min for UV, 78.2% at 80 min under visible light	Hummer's modified method	[77]
$Eu_2SmSbO_7/ZnBiEuO_4$	0.75	11.21	A 500W Xe lamp	88.16 % at 160 min	hydrothermal	[76]
g-$C_3N_4/Fe_3O_4/CuWO_4$/CuO	1.5	10	200 W	93% at 150 min	Multi steps method	This work

References

[1] AbuKhadra, M.R., Mohamed, A.S., El-Sherbeeny A.M., Elmeligy, M.A. (2020), Enhanced photocatalytic degradation of acephate pesticide over MCM-41/Co3O4 nanocomposite synthesized from rice husk silica gel and Peach leaves, *Journal of Hazardous Materials*, 389, 12212. DOI: 10.1016/j.jhazmat.2020.122129.

[2] Makino Y., Oshita S., Murayama Y., Mori M., Kawagoe Y., Sakai K., (2009). Nondestructive Analysis of Chlorpyrifos on Apple Skin Using UV Reflectance. *Transactions of the ASABE (American Society of Agricultural and Biological Engineers)*, 52(6), 1955-1960. DOI: 10.13031/2013.29191.

[3] Patel, V., Rai, M.K., Mundeja, P., Rai, J. (2014). Sensitive Spectrophotometric Determination of Chlorpyrifos in Different Environmental and Biological Samples, *International Journal of Science and Research (IJSR)*, 3(7), 1546-1550.

[4] Rathod, A.L, Garg, R.K. (2017). Chlorpyrifos poisoning and its implications in human fatal cases: A forensic perspective with reference to Indian scenario, *Journal of Forensic and Legal Medicine*, 29-34, DOI: 10.1016/j.jflm.2017.02.003.

[5] Saljooqi, A., Shamspur, T., Mostafavi, A. (2021). Synthesis and photocatalytic activity of porous ZnO stabilized by TiO2 and Fe3O4 nanoparticles: investigation of pesticide degradation reaction in water treatment. *Environmental Science and Pollution Research*, 28, 9146-9156. DOI: 10.1007/s11356-020-11122-2.

[6] Tabasum, S., Sharma, A., Dhupar, N., Bagri, U., Yousuf, S., Kumar, V., Singh, A., Shukla, S.K. (2024).Visible light-induced continuous process for photodegradation of chlorpyrifos using g-C3N4/GO/La2O3 photocatalyst from agricultural aquatic waste, *Chemical Physics Impact*, 9, 1-12, 100751, DOI: 10.1016/j.chphi.2024.100751.

[7] Kgoetlana, C.M., Malinga, S.P., Dlamini, L.N. (2020). Photocatalytic Degradation of Chlorpyrifos with Mn-WO3/SnS2 Heterostructure, *Catalysts*, 10, 1-21, DOI: 10.3390/catal10060699.

[8] Hussein, M.A., Ahmed, D.N., (2025). Efficient nano emulsion Co-stabilized by iron nano oxides coated with graphene slag for removal of Co-trimoxazole, *Journal of the Indian Chemical Society*, 102, 1-8, DOI: 10.1016/j.jics.2024.101538.

[9] Zhou, S., Wang, Y., Zhao, G., Li, C., Liu, L., Jiao, F., (2021) Enhanced visible light photocatalytic degradation of rhodamine B by Z-scheme CuWO4/g-C3N4 heterojunction, *J. Mater. Sci. Mater. Electron*, 32, 2731–2743, DOI: 10.1007/s10854-020-05003-0.

[10] Mohammed, N.A.A., I. Alwared, A., S. Salman, M. (2020). Decolorization of Reactive Yellow Dye by Advanced Oxidation Using Continuous Reactors. *Iraqi Journal of Chemical and Petroleum Engineering*, 21(2), 1–6. DOI: 10.31699/ ijcpe.2020.2.1.

[11] Aziz, K., Naz, A., Manzoor, S., Imran Khan, M., Shanableh, A., Fernandez Garcia, J., (2023). Visible Light Photodegradation of Glyphosate and Methylene Blue Using Defect-Modified Graphitic Carbon Nitride Decorated with Ag/TiO2, *Catalysts*, 13(7), 1-20,. DOI: 10.3390/catal13071087.

[12] Mohsen, D.M., Al-Jubouri, S.M., Al-Batty, S., (2025). Photocatalytic degradation of a cationic dye using Ag2O@CuO nanoellipsoidal photocatalyst under ultraviolet irradiation, *Iraqi Journal of Chemical and Petroleum Engineering*, 26(4), 27–40, DOI: 10.31699/IJCPE.2025.4.3.

[13] Hosseini, N., Toosi, M.R. (2018) Combined adsorption process and photocatalytic degradation of some commercial herbicides over N-doped TiO2 particles supported on recyclable magnetic hexagonal mesoporous silica, *Separation Science and Technology*, 54(11), 1697-1709, DOI: 10.1080/01496395.2018.1539105.

[14] Hameed, F.M., Mousa, K.M. (2019) Study on Kinetic and Optimization of Continuous Advanced Oxidative Decolorization of Brilliant Reactive Red Dye, *Iraqi Journal of Chemical and Petroleum Engineering*, 20(1), 9–14, DOI: 10.31699/IJCPE.2019.1.2.

[15] Xuan, N.T., Nguyen Thi, D., Tran Thuong, Q., Nguyen Ngoc, T., Dang Quoc, K., Molnár, Z., Mukhtar, S., Szabó-Bárdos, E., Horváth, O. (2023). Effect of Copper-Modification of g-C3N4 on the Visible-Light-Driven Photocatalytic Oxidation of Nitrophenols., *Molecules*, 28(23), 1-18, 7810, DOI: 10.3390/molecules28237810.

[16] Abdulrazaq, H.A., Alwared, A.I., Onyeaka, H. (2023). Ibuprofen Degradation from Synthetic Wastewater UsingPhoto-Fenton Process. *Iraqi Journal of Chemical and Petroleum Engineering*, 24(4), 107–114, DOI: 10.31699/IJCPE.2023.4.11.

[17] Mousavi, M., Habibi-Yangjeh, A., Pouran, S.R., (2018) .Review on magnetically separable graphitic carbon nitride-basednanocomposites as promising visible-light-driven photocatalysts, *J. Mater. Sci. Mater. Electron*, 29, 1719–1747, DOI: 10.1007/s10854-017-8166-x.

[18] Askari, N., Beheshti, M., Mowla, D., Farhadian, M. (2020). Fabrication of CuWO4/Bi2S3/ZIF67 MOF: A novel double Z-scheme ternary heterostructure for boosting visible-light photodegradation of antibiotics, *Chemosphere*, 251, 1-18, DOI: 10.1016/j.chemosphere.2020.126453.

[19] Hu, X., Gao, D., Li, Y., Dong, H., Zhou, W., Yang, L., Zhang, Y. (2019) Fabrication of novel CuWO4 nanoparticles (NPs) for photocatalytic degradation of methylene blue in aqueous solution, *SN Applied Sciences*, 1(119), 1-10, DOI: 10.1007/s42452-018-0113-9.

[20] Raizada, P., Sharma, S., Kumar, A., Singh, P., Khan, A.A.P., Asiri, A.M. (2020) Performance improvement strategies of CuWO4 photocatalyst for hydrogen generation and pollutant degradation, *Journal of Environmental Chemical Engineering*, 8(5), 1-82, DOI: 10.1016/j.jece.2020.104230.

[21] Barzgari, Z., Askari, S.Z., Ghazizadeh, A. (2017). Fabrication of nanostructured CuWO4 for photocatalytic degradation of organic pollutants in aqueous solution, *J. Mater. Sci. Mater. Electron*, 1-6, DOI: 10.1007/s10854-016-5922-2

[22] Benabbas, Kh., Zabat, N., Hocini, I. (2020). Facile synthesis of Fe3O4/CuO a core-shell heterostructure for the enhancement of photocatalytic activity under visible light irradiation, *Environmental Science and Pollution Research*, 1-13, DOI: 10.1007/s11356-020-10749-5.

[23] Mamba, N., Makhetha, T.A., Mbuli, B.S., Malinga, S.P. (2025). Synthesis of quantum dot-based CuO/Fe3O4@g-C3N4 dual Z-scheme ternary composite from Aloe vera, *Inorganic Chemistry Communications*, 176, 1-8, DOI: 10.1016/j.inoche.2025.114215.

[24] Zhang, Y., Lian, P., Hao, X., Zhang, L., Yang, L., Jiang, L., Zhang, K., Liao, L., Qin, A. (2025). Modification Strategies of g-C3N4-Based Materials for Enhanced Photoelectrocatalytic Degradation of Pollutants: A Review. *Inorganics*, 13, 1-30. DOI: 10.3390/inorganics13070225.

[25] Li, Y., Zhang, H., Zhang, D.,Yao, S., Dong, S., Chen, Q., Fan, F., Jia,H., Dong, M. (2024). Construction of Bi2WO6/g-C3N4 Z-Scheme Heterojunction and Its Enhanced Photocatalytic Degradation of Tetracycline with Persulfate under Solar Light. *Molecules*, 29(5), 1-15, DOI: 10.3390/ molecules29051169.

[26] Reddy, Ch.V., Nagar, A., Shettic, N.P., Reddy, I.N., Basu, S., Shima, J., Kakarla, R.R., (2023). Novel g-C3N4/BiVO4 heterostructured nanohybrids for high efficiency photocatalytic degradation of toxic chemical pollutants, *Chemosphere*, 322, 1-10, DOI: 10.1016/j.chemosphere.2023.138146.

[27] Patra, R.; Dash, P., Panda, P.K., Yang, P.-C. (2023). A Breakthrough in PhotocatalyticWastewater Treatment: The Incredible Potential of g-C3N4/Titanate Perovskite-Based Nanocomposites. *Nanomaterials*, 13 (2173), 1-32. DOI: 10.3390/nano13152173.

[28] Suresh, R., Karthikeyan, N.S., Gnanasekaran, L., Rajendran, S., Soto-Moscoso, M. (2023). Facile synthesis of CuO/g-C3N4 nanolayer composites with superior catalytic reductive degradation behavior, *Chemosphere*, 315, 1-12, DOI: 10.1016/j.chemosphere.2022.137711.

[29] Atri, A., Echabaane, M., Bouzidi, A., Harabi, I., Soucase, B.M., Chaabane, R.B. (2023) .Green synthesis of copper oxide nanoparticles using Ephedra Alata plant extract and a study of their antifungal, antibacterial activity and photocatalytic performance under sunlight, *Heliyon*, 9, 1-16, DOI: 10.1016/j.heliyon.2023.e13484

[30] Wang, L., Ma, X., Huang, G., Lian, R., Huang, J., She, H., Wang, Q. (2022) .Construction of ternary CuO/CuFe2O4/g-C3N4 composite and its enhanced photocatalytic degradation of tetracycline hydrochloride with persulfate under simulated sunlight, *Journal of Environmental Sciences*, 112, 59–70, DOI: 10.1016/j.jes.2021.04.026.

[31] Jayasimha, H.N., Chandrappa, K.G., Sanaulla, P.F., Dileepkumar, V.G. (2024) . Green synthesis of CuO nanoparticles: A promising material for photocatalysis and electrochemical sensor, *Sensors International*, 5, 1-10, DOI: 10.1016/j.sintl.2023.100254.

[32] Nazim, M., Khan, A.A.P., Asiri, A.M., Kim, J.H. (2021). Exploring Rapid Photocatalytic Degradation of Organic Pollutantswith Porous CuO Nanosheets: Synthesis, Dye Removal, and Kinetic Studies at Room Temperature, *ACS Omega*, 6, 2601−2612, DOI: 10.1021/acsomega.0c04747

[33] Yadav, M., Shukla, A.K., Srivastva, N., Upadhyay, S.N., Dubey, S.K. (2015). Utilization of microbial community potential for removal of chlorpyrifos:a review, *Crit. Rev. Biotechnol*., 1-16, DOI: 10.3109/07388551.2015.1015958.

[34] Ali, S.M., Alwared, A.I. (2026). Photocatalytic degradation of Glyphosate by g-C3N4 /Fe3O4/CuWO4/CuO type Z– scheme heterojunction: Synthesis, characterization, mechanism studies and reusability, *Desalination and Water Treatment*, 325, 1-18, DOI: 10.1016/j.dwt.2025.101574

[35] Li, H., Li, N, Wang, M, Zhao, B., Long, F. (2018). Synthesis of novel and stable g-C3N4-Bi2WO6 hybrid nanocomposites and their enhanced photocatalytic activity under visible light irradiation. *R. Soc. Open Sci*., 5, 1-12. DOI: 10.1098/rsos.171419.

[36] Wang, X., Lizong, D. (2018). Well-dispersed zero-valent iron supported on Fe3O4/g-C3N4 composites via a facile approach with versatile photoredox catalysis, *Journal of Nanoparticle Research*, 20(12), 1-13, DOI: 10.1007/s11051-018-4401-5.

[37] Chen, H., Leng, W., Xu, Y. (2014). Enhanced Visible-Light Photoactivity of CuWO4 through a Surface-Deposited CuO. *J. Phys. Chem. C*, 118, 9982−9989, DOI: 10.1021/jp502616h.

[38] Arulkumar, E., Thanikaikarasan, S. (2024). Structural feature, morphology and optical properties of g-C3N4 decorated CuO-Fe3O4 nano composite for electrocatalytic and photocatalytic applications, *Diamond and Related Materials*, 147, 111-294, DOI: 10.1016/j.diamond.2024.111294.

[39] Sharma, R., Islam, N., Priye, A., Singh, J., Kumar, M., Kumar, D., Sharma, P.P., Chauhan, V., Shandilya, P. (2024) .Fabrication of dual S-scheme based CuWO4/NiFe/WO3 heterojunction for visible-light-induced degradation and reduction applications, *Journal of Environmental Chemical Engineering*, 12(2), 1-17, DOI: 10.1016/j.jece.2024.112126.

[40] Zhu, D.L., Liu, S., Chen, M., Zhang, J., Wang, X. (2017). Flower-like-flake Fe3O4/g-C3N4 nanocomposite: facile synthesis, characterization, and enhanced photocatalytic performance, *Colloids and Surfaces A: Physicochemical and Engineering Aspects*, 372-382, DOI: 10.1016/j.colsurfa.2017.10.053.

[41] Habibi-Yangjeh, A., Mousavi, M., Nakata, K. (2018). Boosting visible-light photocatalytic performance of g-C3N4/Fe3O4 anchored with CoMoO4 nanoparticles: Novel magnetically recoverable photocatalysts, *Journal of Photochemistry and Photobiology, A: Chemistry*, 368, 120-136, DOI: 10.1016/j.jphotochem.2018.09.026.

[42] Che, H., Liu, C., Hu, W., Hu, H., Li, J.Q., Dou, JY., Shi, W.D., Li, C., Dong, H. (2017). NGQDs active sites as effective collectors of charge carriers for improving photocatalytic performance of Z-scheme gC3N4/Bi2WO6 heterojunctions under Vis- and NIR-light, *Catal. Sci. Technol.*, 622-631, DOI: 10.1039/C7CY01709J.

[43] Mukhtar, S., Szabó-Bárdos, E., Oze, C., Juzsakova, T., Rácz, K., Németh, M., Horváth, O. (2025). g-C3N4 Modified with Metal Sulfides for Visible – Light - Driven Photocatalytic Degradation of Organic, *Pollutants.Molecules*, 30, 1-28, DOI: 10.3390/molecules30020253.

[44] Liu, D., Lu, C., Wu, J. (2018) CuO/g-C3N4 nanocomposite for elemental mercury capture at low temperature,(2018). *J. Nanopart. Res.*, 20(277), 1-11, DOI: 10.1007/s11051-018-4374-4.

[45] Sun, M., Zeng, Q., Zhao, X., Shao, Y., Ji, P., Wang, C., Yan, T., Du, B. (2017). Fabrication of novel gC3N4 nanocrystals decorated Ag3PO4 hybrids: Enhanced charge separation and excellent visible-light driven photocatalytic activity, *Journal of Hazardous Materials*, 9-21, DOI: 10.1016/j.jhazmat.2017.06.003.

[46] My Hang, T.T., Thao Vy, N.H., Hanh, N.T., Pham, T.-D., Hoang Yen, L.T. (2021). Facile synthesis of copper tungstate (CuWO4) for novel photocatalytic degradation of tetracycline under visible light. *Sustainable Chemistry and Pharmacy*, 21, 1-13, 100407. DOI: 10.1016/j.scp.2021.100407.

[47] Vinesh, V., Preeyanghaa, M., Naveen Kumar, T.R., Ashokkumar, M., Bianchi, L., Neppolian, B. (2022) .Revealing the stability of CuWO4/g-C3N4 nanocomposite for photocatalytic tetracycline degradation from the aqueous environment and DFT analysis, *Environmental Research*, 207, 1-11, DOI: 10.1016/j.envres.2021.112112.

[48] Habibi-Yangjeh, A., Mousavi, M. (2018). Deposition of CuWO4 nanoparticles over g-C3N4/Fe3O4 nanocomposite: Novel magnetic photocatalysts with drastically enhanced performance under visible-light, *Advanced Powder Technology*, 29(6), 1379-1392, DOI: 10.1016/j.apt.2018.02.034.

[49] Ali, A.H., Alwared, A.I. (2024). Construction of ternary heterostructure of zeolite/Fe3O4/CuS/CuWO4 as a reusable: Characterization studies, *Asia-pacific Journal of Chemical Engineering*, 19(5), DOI: 10.1002/apj.3125.

[50] Hong, S., Yu, Y., Yi, Z., Zhu, H., Wu, W., Ma, P. (2016). Highly Efficient and Recyclable g-C3N4/CuO Hybrid Nanocomposite Towards Enhanced Visible-Light Photocatalytic Performance, *Nano: Brief Reports and Reviews*, 11(11), 1-19, 1650121, DOI: 10.1142/S1793292016501216.

[51] Saadati, M., Akhavan, O., Fazli, H. (2021). Single-Layer MoS2-MoO3-x Heterojunction Nanosheets with Simultaneous Photoluminescence and Co-Photocatalytic Features. *Catalysts*, 11, DOI: 10.3390/catal11121445.

[52] Okab, A.A., Alwared, A.I. (2023) Photodegradation of tetracycline antibiotic by ternary recyclable Z-scheme g-C3N4/Fe3O4/Bi2WO6/Bi2S3 photocatalyst with improved charge separation efficiency: Characterization and mechanism studies, *Environmental Nanotechnology, Monitoring & Management*, 19, 1-18, DOI: 10.1016/j.enmm.2022.100767.

[53] Abass, I.S., Alwared, A.I. (2025). Synthesis, Characterization of S-Scheme Heterojunction (rGO/Fe3O4/Bi2S3/MgZnO) for Enhance Photocatalytic Degradation of Sulfonylurea Herbicides Under Visible Light, *Water Air Soil Pollut.*, 236(248), 1-22, DOI: 10.1007/s11270-025-07879-2.

[54] Mohamad, V.I., Alwared, A.I. (2025) Bio-enhanced photocatalytic removal of black azo dye from aqueous solutions using g-C3N4/Fe3O4/Ag2O nanocomposites under visible light, *Journal of Taibah University for Science*, 19(1), 1-19, DOI: 10.1080/16583655.2025.2463791.

[55] Shokoohi, R., Khazaei, M., Godini, K., Azarian, G., Latifi, Z., Javadimanesh, L., Nasab, H.Z. (2021). Degradation and mineralization of methylene blue dye by peroxymonosulfate/Mn3O4 nanoparticles using central composite design: Kinetic study, *Inorganic Chemistry Communications*, 127, 1-14, DOI: 10.1016/j.inoche.2021.108501.

[56] Adday, A.S., Al-Jubouri, S.M., Al-Batty, S. (2025). Photocatalytic degradation of methylene blue by robust visible-light-driven polyvinylidene fluoride membranes incorporating Ag2O@CRA photocatalyst: Kinetics analysis and cost assessment. *Iraqi Journal of Chemical and Petroleum Engineering*, 26(3), 19-28, DOI: 10.31699/IJCPE.2025.3.3.

[57] Elhalil, A. , Elmoubarki, R., Sadiq, M., Abdennouri, M., Kadmi, Y., Favier, L., Qourzal, S., Barka, N. (2017). Enhanced photocatalytic degradation of caffeine as a model pharmaceutical pollutant by Ag-ZnO-Al2 O3 nanocomposite, *Desalination and Water Treatment*, 94, 254–262, DOI: 10.5004/dwt.2017.21587.

[58] Nezamzadeh-Ejhieh, A., Hushmandrad, S., (2010). Solar photodecolorization of methylene blue by CuO/X zeolite as a heterogeneous catalyst, *Applied Catalysis A: General*, 388, 149–159, DOI: 10.1016/j.apcata.2010.08.042.

[59] Amakiri, K.T., Angelis-Dimakis, A., Canon, A.R. (2021). Recent advances, influencing factors, and future research prospects using photocatalytic process for produced water treatment, *Water Science & Technology*, 85(3), 769, DOI: 10.2166/wst.2021.641.

[60] Soltani-nezhad, F., Saljooqi, A., Mostafavi, A., Shamspur, T. (2019).Synthesis of Fe3O4/CdS–ZnS nanostructure and its application for photocatalytic degradation of chlorpyrifos pesticide and brilliant green dye from aqueous solutions, *Ecotoxicology and Environmental Safety*, 189, 1-12. DOI: 10.1016/j.ecoenv.2019.109886.

[61] Nekooie, R., Shamspur, T., Mostafavi, A. (2020). Novel CuO/TiO2/PANI nanocomposite: Preparation and photocatalytic investigation for chlorpyrifos degradation in water under visible light irradiation, *Journal of Photochemistry and Photobiology, A: Chemistry*, 407, 1-37, DOI: 10.1016/j.jphotochem.2020.113038.

[62] Bruckmann, F.S., Schnorr, C., Oviedo, L.R., Knani, S., Silva, L.F.O., Silva, W.L., Dotto, G.L., Bohn Rhoden, C.R. (2022). Adsorption and Photocatalytic Degradation of Pesticides into Nanocomposites: A Review, *Molecules*, 27, 6261. DOI: 10.3390/molecules27196261.

[63] Muhammed, S.M.A., Al-Qaisi, A.Z., Al Yousif, M.A., Alkadhim, N. (2024). Using Eucalyptus Peels as a Permeable Reactive Barrier for Treating Groundwater Contaminated with Copper Ions – A Simulation with COMSOL Software, *Journal of Ecological Engineering*, 25(11), 37–45, DOI: 10.12911/22998993/192637.

[64] Raeisi-Kheirabadi, N., Nezamzadeh-Ejhieh, A. (2020). A Z-scheme g-C3N4/Ag3PO4 nanocomposite: Its photocatalytic activity and capability for water Splitting, *International Journal of Hydrogen Energy*, 45(58), 1-13. DOI: 10.1016/j.ijhydene.2020.09.028.

[65] Hanha, N.T., Trib, N.L.M., Thuand, D.V., Tung, M.H.T., Phamg, T.-D., Tran Minhi, D., Trang, H.T., Binh, M.T., Nguyen, M.V. (2019). Monocrotophos pesticide effectively removed by novel visible light driven Cu doped ZnO photocatalyst, *Journal of Photochemistry & Photobiology A: Chemistry*, 382, 111923, DOI: 10.1016/j.jphotochem.2019.111923.

[66] Shirzad-Siboni, M., Jonidi-Jafari, A., Farzadkia, M., Esrafili, A., Gholami, M. (2016). Enhancement of photocatalytic activity of Cu-doped ZnO nanorods for the degradation of an insecticide: Kinetics and reaction pathways, *Journal of Environmental Management*, 186, Part 1, 1-11, DOI: 10.1016/j.jenvman.2016.10.049.

[67] Redha, Z.M., Yusuf, H.A., Amin, R., Bououdina, M. (2020). The study of photocatalytic degradation of a commercial azo reactive dye in a simple design reusable miniaturized reactor with interchangeable TiO2 nanofilm, *Arab Journal of Basic and Applied Sciences*, 27(1), 287-298, DOI: 10.1080/25765299.2020.1800163.

[68] Luan, Ji., Shen, Y., Zhang, L., Guo, N. (2016). Property Characterization and Photocatalytic Activity Evaluation of BiGdO3 Nanoparticles under Visible Light Irradiation, *Int. J. Mol. Sci*., 17, 1441, DOI: 10.3390/ijms17091441 .

[69] Sin, J.-C., Lam, S.-M., Zeng, H., Lin, H., Li, H., Kumaresan, A.K., Mohamed, A.R., Lim, J.-W. (2020). Z-scheme heterojunction nanocomposite fabricated by decorating magnetic MnFe2O4 nanoparticles on BiOBr nanosheets for enhanced visible light photocatalytic degradation of 2,4-dichlorophenoxyacetic acid and Rhodamine B. *Separation and Purification Technology*, 250, 117186, DOI: 10.1016/j.seppur.2020.117186.

[70] Khan, M.,, Ahmed, M.M., Akhtar, M.N., Sajida, M., Riaz, N.N., Asif, M., Muhammad, K., Shabbir, B., Ahmad, K., Saeed, M., Shafiq, M., Shabir, T. (2024) Fabrication of CuWO4@MIL-101 (Fe) nanocomposite for efficient OER and photodegradation of methylene blue, *Heliyon*, 10, DOI: 10.1016/j.heliyon.2024.e40546.

[71] Ali, S.M., Alwared, A.I. (2026). Photocatalytic Detoxification of Glyphosate herbicide in Water using Visible-Light Active over g-C3N4/Fe3O4/CuWO4/CuO Nanocomposites, *South African Journal of Chemical Engineering*, 1-17, DOI: 10.1016/j.sajce.2026.100865.

[72] Ayodhya, D., Veerabhadram, G. (2016). Ternary semiconductor ZnxAg1-xS nanocomposites for efficient photocatalytic degradation of organophosphorus pesticides, *Photochemical & Photobiological Sciences*, 15(3), 311–458, DOI: 10.1039/C8PP00220G.

[73] Farrukh, M.A., Butt, K.M., Chong, K-K., Chang, W.S. (2019). Photoluminescence emission behavior on the reduced band gap of Fe doping in CeO2-SiO2nanocomposite and photophysical properties, *Journal of Saudi Chemical Society*, 23, 561–575, DOI: 10.1016/j.jscs.2018.10.002.

[74] Merci, S., Saljooqi, A., Shamspur, T., Mostafavi, A. (2020). Investigation of photocatalytic chlorpyrifos degradation by a new silica mesoporous material immobilized by WS2 and Fe3O4 nanoparticles: Application of response surface methodology. *Appl. Organomet. Chem*., 1–14, DOI: 10.1002/aoc.5343.

[75] Rashidimoghaddam, M., Saljooqi, A., Shamspur, T., Mostafav, A. (2020). Constructing S-doped Ni–Co LDH intercalated with Fe3O4 heterostructure photocatalysts for enhanced pesticide degradation, *New J. Chem.*, 15584-15592, DOI: 10.1039/d0nj02772c.

[76] Rani, M., Yadav, J., Keshu Shanker, U. (2021). Green synthesis of sunlight responsive zinc oxide coupled cadmium sulfide nanostructuresfor efficient photodegradation of pesticides. *J. Colloid Interface Sci.* 601, 689–703, DOI: 10.1016/j.jcis.2021.05.152.

[77] Esfandian, H., Mirzaei, S., Chari, A.S., Ghadi, R.A., Moqadam, I.H. (2023). Photocatalytic degradation of chlorpyrifos pesticide in aqueous solution using Cu-doped TiO2/GO photocatalysis vicinity of UV and visible light, *Research Square*, 35, 1-16, DOI: 10.21203/rs.3.rs-3057094/v1.

[78] Luan, J., Wang, Y., Yao, Y., Hao, L., Li, J., Cao, Y. (2024). Preparation and Property Characterization of Eu2SmSbO7/ZnBiEuO4 Heterojunction Photocatalysts and Photocatalytic Degradation of Chlorpyrifos under Visible Light Irradiation, *Catalysts*, 14(2), 1-32, DOI: 10.3390/catal14020144.